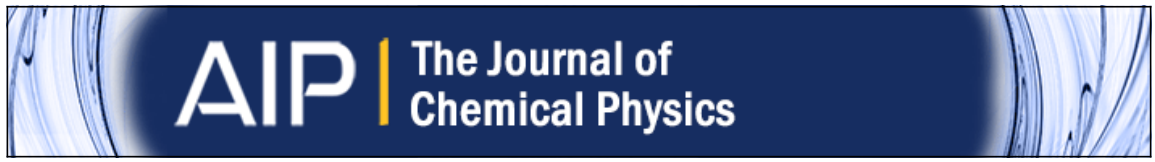

Fluorescencedetected wave packet interferometry: Time resolved molecular spectroscopy with sequences of femtosecond phaselocked pulses

Norbert F. Scherer, Roger J. Carlson, Alexander Matro, Mei Du, Anthony J. Ruggiero, Victor Romero Rochin, Jeffrey A. Cina, Graham R. Fleming, and Stuart A. Rice

Citation: The Journal of Chemical Physics **95**, 1487 (1991); doi: 10.1063/1.461064
View online: http://dx.doi.org/10.1063/1.461064
View Table of Contents: http://scitation.aip.org/content/aip/journal/jcp/95/3?ver=pdfcov
Published by the AIP Publishing

Articles you may be interested in

Preparation and resolution of molecular states by coherent sequences of phase-locked ultrashort laser pulses
J. Chem. Phys. **121**, 2117 (2004); 10.1063/1.1767513

Wave packet interferometry without phase-locking
J. Chem. Phys. **108**, 6057 (1998); 10.1063/1.476501

Phaselocked detection of fluorescence lifetime
Rev. Sci. Instrum. **64**, 2531 (1993); 10.1063/1.1143915

Fluorescencedetected wave packet interferometry. II. Role of rotations and determination of the susceptibility
J. Chem. Phys. **96**, 4180 (1992); 10.1063/1.462837

Time resolved dynamics of isolated molecular systems studied with phaselocked femtosecond pulse pairs
J. Chem. Phys. **93**, 856 (1990); 10.1063/1.459456

This article is copyrighted as indicated in the article. Reuse of AIP content is subject to the terms at: http://scitation.aip.org/termsconditions. Downloaded to IP: 128.32.208.2 On: Thu, 29 May 2014 17:58:57

Fluorescence-detected wave packet interferometry: Time resolved molecular spectroscopy with sequences of femtosecond phase-locked pulses

Norbert F. Scherer,[a] Roger J. Carlson, Alexander Matro, Mei Du, Anthony J. Ruggiero,[b] Victor Romero-Rochin,[c] Jeffrey A. Cina, Graham R. Fleming, and Stuart A. Rice

Department of Chemistry and The James Franck Institute, The University of Chicago, Chicago, Illinois 60637

(Received 31 December 1990; accepted 24 April 1991)

We introduce a novel spectroscopic technique which utilizes a two-pulse sequence of femtosecond duration phase-locked optical laser pulses to resonantly excite vibronic transitions of a molecule. In contrast with other ultrafast pump–probe methods, in this experiment a definite optical phase angle between the pulses is maintained while varying the interpulse delay with interferometric precision. For the cases of in-phase, in-quadrature, and out-of-phase pulse pairs, respectively, the optical delay is controlled to positions that are integer, integer plus one quarter, and integer plus one half multiples of the wavelength of a selected Fourier component. In analogy with a double slit optical interference experiment, *the two pulse experiments reported herein involve the preparation and quantum interference of two nuclear wave packet amplitudes* in an excited electronic state of a molecule. These experiments are designed to be sensitive to the total phase evolution of the wave packet prepared by the initial pulse. The direct determination of wave packet phase evolution is possible because phase locking effectively transforms the interferogram to a frame which is referenced to the optical carrier frequency, thereby eliminating the high (optical) frequency modulations. This has the effect of isolating the rovibrational molecular dynamics. The phase locking scheme is demonstrated for molecular iodine. The excited state population following the passage of both pulses is detected as the resultant two-beam dependent fluorescence emission from the B state. The observed signals have periodically recurring features that result from the vibrational dynamics of the molecule on the electronically excited potential energy surface. In addition, coherent interference effects cause the magnitude and sign of the periodic features to be strongly modulated. The two-pulse phase-locked interferograms are interpreted herein by use of a simple analytic model, by first order perturbation theory and by quantum mechanical wave packet calculations. We find the form of the interferogram to be determined by the ground state level from which the amplitude originates, the deviation from impulsive preparation of the wave packet due to nonzero pulse duration, the frequency and anharmonicity of the target vibrational levels in the B state, and the detuning of the phase-locked frequency from resonance. The dependence of the interferogram on the phase-locked frequency and phase angle is investigated in detail.

I. INTRODUCTION

The achievement of selective control of product formation in a reaction has been sought persistently throughout the evolution of chemistry. To date, such control has only been accomplished at the macroscopic level, by manipulation of external variables such as temperature, pressure, solvent character, etc. Recent theoretical work has shown that it is, in principle, possible to influence the selectivity of product formation by intervention at the microscopic level, by controlling the molecular dynamics. Brumer and Shapiro[1] have shown that control of product selectivity can be achieved if two degenerate exit channel wave functions can be made to interfere constructively or destructively by the simultaneous generation of two or more coherent excitation routes to the degenerate final states. The technical implementation of this method requires controlling the phase difference between the two cw laser sources driving the different excitation routes. Tannor and Rice,[2] and Tannor, Kosloff, and Rice,[3] have shown that controlling the duration of propagation of a wave packet on an excited state electronic potential energy surface, by controlling the time delay between pump and dump pulses, can be used to influence the selectivity of products formed on the ground state potential energy surface; greater selectivity results if both the phase structure of the pulses and the time delay between them are controlled. The development of a technique to control both the temporal separation of the pulses and the relative phases

[a] National Science Foundation Postdoctoral Fellow.

[b] Permanent address: Lawrence Livermore National Laboratory, Livermore, California 94550.

[c] Permanent address: Instituto de Fisica, Universidad Nacional Autonoma de Mexico, Apartado Postal 20-364, 01000 Mexico, D. F., Mexico.

This article is copyrighted as indicated in the article. Reuse of AIP content is subject to the terms at: http://scitation.aip.org/termsconditions. Downloaded to IP: 128.32.208.2 On: Thu, 29 May 2014 17:58:57

of the pulses at the optical carrier frequency has important implications for the implementation of this method.

Rabitz and co-workers[4] have shown that it is possible to design optimally shaped pulses that will guide the evolution of a system from a chosen initial state to a selected final state in a specified time interval. Their work, which has been applied only to reactions on one potential energy surface, has been extended by Kosloff, Rice, Gaspard, Tersigni, and Tannor[5] to the design of optimally shaped pulses that utilize modulation of wave packet evolution on an excited state potential energy surface to influence the selectivity of product formation on the ground state potential energy surface. The implementation of this method requires further development of femtosecond pulse shaping technology, as exemplified by the work of Heritage *et al.*[6] and Warren and coworkers.[7]

This paper reports the development of a method for setting and maintaining control of the relative phases of sequences of femtosecond duration optical pulses.[8] The method of achieving phase control of pulses which we report is applicable at all optical wavelengths and for pulse separations less than 25 ps. A significant aspect of the technique is the requirement for only 1 part in 10^4 accuracy in knowledge of the optical carrier frequency to obtain phase-locked wave forms for these time intervals. Actually, only the relative phase of a selected bandpass of the pulse spectrum, termed the locked frequency, is maintained at a constant value; the spectral width of that bandpass is 0.67 or 1.00 cm^{-1} in our experiments. For the case of transform limited pulses, the relative phases of the other Fourier components of the pulses outside the locked bandwidth are determined as the product of the detuning from the locked frequency and the time separation of the pulses. We describe the preparation of pairs of optical pulses locked in phase, but generalization to more complicated multiple pulse sequences with all conceivable relative phases ($\phi = 0, \pi/2, \pi/4$) is possible. The application of the phase-locked pulse pair methodology to generate the transient fluorescence-detected interference dynamics of I_2 is treated in detail.

It is appropriate to emphasize that the application of phase control which we report, namely a study of the transient fluorescence interferogram from I_2, is a form of interference spectroscopy. In the I_2 experiments the first pulse of a two-pulse sequence transfers probability amplitude from the electronic ground state, forming a "replica" of the ground state vibrational wave function; that replica evolves as a wave packet on the excited state potential energy surface during the time interval between pulses. The second pulse of the sequence, whose phase is locked to that of the first one, also creates a wave packet in the excited electronic state, which is in superposition with the initial, propagated, wave packet. The average excited state population is determined after the second pulse by measuring the total fluorescence from a collection of identically driven molecules. The situation is analogous to a two slit experiment in that the excited state amplitude in each molecule is the sum of the excitation amplitudes generated by two routes which are not distinguished from each other by measurement. Such an intramolecular superposition of amplitudes can lead to interference. Whether the interference is constructive or destructive, giving rise to larger or smaller excited state population for a given interpulse delay, depends on the optical phase difference between the two pulses and on the detailed nature of the evolution of the initial wave packet. In particular, it depends on the wave packet's time-dependent quantum mechanical phase.

The nature of the interference effects induced by the phase-locked pulse pair can be understood, equivalently, as follows. The phase-locked probe pulse may be viewed as a reference clock with which the evolution of the initial coherent superposition state is compared. The initially prepared coherent superposition state consists of a Franck–Condon factor weighted sum of excited state vibrational eigenfunctions, each having a time dependent phase with an initial condition determined by the phase of the corresponding frequency component of the first pulse. A single frequency component of the second pulse, the locked frequency, is maintained with a 0, 90, or 180 deg phase shift with respect to the identical frequency Fourier component of the initial pulse. For a given temporal pulse separation, the relative phases of the other spectral components depend on their detunings from the locked frequency. Therefore, the second pulse creates a superposition state in which each of the eigenfunction components has a well defined phase, differing from the accumulated phase of that eigenfunction in the first superposition state by an amount depending on the difference between the vibronic transition energy and the locked frequency[9] for a given temporal delay. The combined excited state amplitudes interfere with each other to an extent determined by these same quantities as well as by the selected relative phase angle of the pulses.

By monitoring the polarization induced in the sample by the initial laser pulse, one could completely determine the linear (and higher order nonlinear) response of the system to an external field. Since we have been concerned with driving an electronic transition which has a large transition frequency, *direct* phase sensitive measurement of the optical free induction decay has not yet been performed. However, measurement of the average excited state population generated by phase-locked pulse pairs is actually equivalent to determination of the time dependent linear polarization.[10] This method of population detection determines the first order frequency dependent susceptibility in the vicinity of the locked frequency component with a range given by the spectral width of the laser pulses. By combining the data from in-phase and in-quadrature phase-locked fluorescence interferograms it is possible to directly obtain both the real (dispersive) and imaginary (absorptive) contributions to the linear response without Kramers–Kronig inversion of the data. We have completed measurements of the in-quadrature fluorescence interferogram of I_2 and will report those data and associated calculations in another paper.

The technique and experiment we describe below are different from the pump–probe measurements recently reported by Gerdy, Dantus, Bowman, and Zewail.[11] These investigators showed that by varying the time between two pump pulses and probing the excited state population with a third pulse they could "control" the population of the *B* state

This article is copyrighted as indicated in the article. Reuse of AIP content is subject to the terms at: http://scitation.aip.org/termsconditions. Downloaded to IP: 128.32.208.2 On: Thu, 29 May 2014 17:58:57

of I_2. However, they did not lock the phases of the pulses at the optical carrier frequency, instead adjusting only the time delay between pulses and, in effect, averaging over the phase difference between the two pump pulses. Their experiment is sensitive to the total time dependent vibrational coordinate distribution of population generated by the separation actions of the two pulses but not to the interference between the amplitudes of the two excited state wave packets which they prepare.

We also call the reader's attention to a recent theoretical study, by Metiu and Engel,[12(a),12(b)] which analyzes a class of experiments related to those described in this paper. They report the results of numerical calculations demonstrating some of the effect of phase control on the two-pulse photodissociation yield of NaI. In addition, they provide an interesting discussion of the analogy between multiple slit scattering phenomena and multiple pulse excitation with phase control. Previous theoretical work on the interference effects of phase controlled optical pulses has also been reported by Villaeys and Freed.[12(c)] Their interest was in the enhancement of quantum beats which can occur when a system absorbs a single photon from a coherent pair of pulses.

Finally, it is important to note that there have been several previously reported experiments which have employed some form of reference stabilized interferometer to carry out measurements with phase-related pulses. Salour,[13] for example, employed a HeNe laser to set the relative phase of two pulses at fixed time delays to demonstrate two-photon optical Ramsey fringe spectroscopy. Diels and co-workers[14] have examined the effect of phase-stabilized multiple pulse excitation on the efficiency and dynamics of multiphoton excitation. Fayer and co-workers[15] have used phase-related pulses to measure the free induction decay of sodium vapor on a time scale of tens of picoseconds.

This paper is organized as follows. Sections II and III contain a description of the laser system and the phase-locking apparatus. The use of a phase-locked pulse pair to obtain the fluorescence-detected interferogram of iodine vapor is then described, along with the experimental results. Section IV contains an analysis of the physical origin of the fluorescence interferogram. We report both analytic results, from a study of a model system whose two displaced electronic potential energy curves support harmonic oscillator motion, and numerical results, from a study of the I_2 system using the known potential energy curves of the X and B electronic states. In Sec. V we compare the experimental and theoretical results, and relate the features of phase-locked pulse pair spectroscopy to other forms of Fourier transform spectroscopy.

II. EXPERIMENTAL DETAILS

A. Laser system

The important characteristics of the phase-locking apparatus will be discussed in the following text. A more detailed description of the lasers and apparatus developed for the experiments reported in this paper is presented elsewhere.[16,17]

The apparatus used in these phase-locked two-pulse experiments employs a mode locked Nd:YAG laser, a femtosecond pulse dye laser and, in the case of dispersed fluroescence measurements, a 100 kHz regenerative amplifier.[17] The mode locked Nd:YAG laser serves as the primary oscillator; it produces a 76 MHz train of 60 ps FWHM pulses with 15 W average power at 1.064 μm. The output of this laser is focussed into a temperature regulated 5 mm long potassium titanyl phosphate (KTP) doubling crystal which is cut for type II phase matching to produce a 1.2 W beam at 532 nm. The 532 nm pulses, of approximately 40 ps FWHM duration, synchronously pump an antiresonant ring dye laser of a new design, in which a cavity dumper serves as the output coupling element.[16] The dumped pulses have an energy of 2–3 nJ, are 50–70 fs FWHM in duration and have a center wavelength in the range of 608–613 nm. The cavity dumping rate was typically 500 kHz for the experiments reported. The associated laser spectra have symmetric near Gaussian or slightly asymmetric distributions of intensity, dependent on the net intracavity group velocity dispersion. An adjustable intracavity slit located at the center of a four prism sequence serves to bias the dye laser pulse forming mechanism to a spectrally limited regime of operation.[18]

B. Experimental arrangement and optical phase-locked loop

The pulses from the dye laser pass through a pair of SF-10 prisms in a double-pass near retroreflecting geometry that serves to compensate for the positive group velocity dispersion of the transmissive optical elements located before the sample cell. The precompensated pulses are injected into a Michelson or Mach–Zehnder interferometer, one arm of which is varied in length by a stepper motor driven optical delay line with 0.1 μm resolution. The other arm of the interferometer contains a retroreflecting mirror mounted on a piezoelectric transducer (PZT) which is used to control the difference in length, hence also the phase difference, between the two arms via a phase-locked loop to be described below. A dual frequency mechanical chopper, with one set of slots positioned in each arm of the interferometer, is used in a double amplitude-modulation configuration for detection of the two-beam-only fluorescence.

The two beams are recombined to propagate collinearly through the sample cell. The combined beams are focused by a spherical mirror (25 cm radius of curvature) through a 75 μm pinhole that facilitates alignment of the interferometer and also maintains phase uniformity of the laser beam wave front. The beam out of the pinhole is recollimated with a spherical mirror, and 90% is reflected and focused with a 20 cm focal length lens into a 5 cm long, room temperature, iodine vapor cell (0.25 Torr vapor pressure). Fluorescence from the iodine vapor is detected, in a right angle geometry, with $f/2$ collection and imaging optics, by a photomultiplier tube (Hammamatsu 649). The output of the photomultiplier tube (PMT) is processed by a lock-in amplifier that is referenced to the sum frequency of both sets of slots of the mechanical chopper. Dual frequency amplitude modulation and phase sensitive detection eliminates both of the single-beam induced-fluorescence signals from contributing to the

This article is copyrighted as indicated in the article. Reuse of AIP content is subject to the terms at: http://scitation.aip.org/termsconditions. Downloaded to IP: 128.32.208.2 On: Thu, 29 May 2014 17:58:57

recorded signal. The two-beam fluorescence signal is recorded for each position of the stepper delay and stored in a computer. The interferometer, experimental arrangement, phase-locked loop (PLL) electronics and signal detection electronics are illustrated in Fig. 1.

The 10% beam intensity transmitted by the beamsplitter is used to detect and set the relative phase of the optical pulses by means of optical interference for time delays nearly 1000 times the pulse duration. This is accomplished as follows. The transmitted portion of the recollimated beam out of the pinhole is expanded ($\times 5$) with spherical achromatic lenses and focused with an $f/5$ lens into a 0.34 m $f/4.5$ monochromator. The beam expansion and f number matching are necessary to properly fill the grating of the monochromator and thus obtain the maximum geometric (i.e., temporal) dispersion.[19] The linear dispersion of the monochromator produces a temporally broadened pulse that is reimaged at the exit slit. The geometrically broadened pulse duration is estimated[19] to be more than 50 ps. The diffraction gratings used in the monochromator had either 1200 or 1800 g/mm so that, with the entrance and exit slits set at 50 μm, the maximum first order spectral resolution was, respectively, 1.00 or 0.67 cm^{-1} (triangular basewidth). The 1.00 cm^{-1} bandpass was centered at a selected frequency, termed

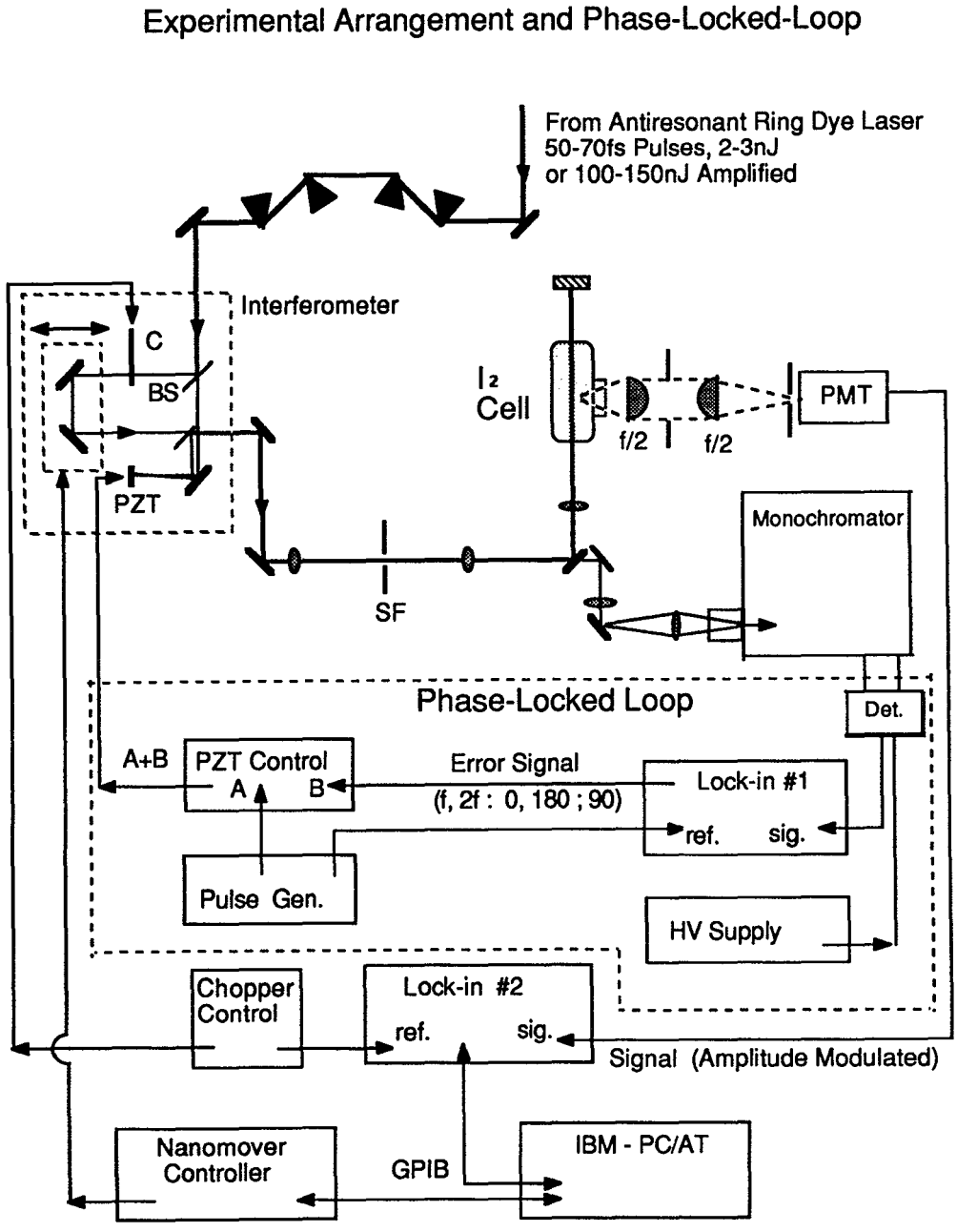

FIG. 1. Schematic of the optical arrangement, the phase-locked loop for stabilization of the interferometer, and the signal detection and processing electronics. C—dual beam chopper, BS—50% beam splitter and recombimer, SF—spatial filter, PMT—photomultiplier tube, Det—photomultiplier tube, PZT—piezoelectric transducer.

This article is copyrighted as indicated in the article. Reuse of AIP content is subject to the terms at: http://scitation.aip.org/termsconditions. Downloaded to IP: 128.32.208.2 On: Thu, 29 May 2014 17:58:57

the locked frequency, and was detected by a second PMT, whose signal is processed by a second lock-in amplifier.

The operation of the phase-locked loop requires a collinear experimental geometry since both beams must travel along the same path through the monochromator and the sample (gas) cell. The collinear geometry causes the output light intensity I from a Michelson (or Mach–Zehnder) interferometer to be given by[20]

$$I = I_0(1 + \cos \Gamma), \tag{2.1}$$

where the accumulated phase $\Gamma = 2\pi l/\lambda$ and l is the difference in optical path length of the two arms of the interferometer. This equation is valid for all path differences for cw light sources. In the present experiment the temporal delay between the pulses t_d, is given by

$$t_d = \{2\pi(N + \delta n) + \phi\}/\Omega_L, \tag{2.2}$$

where Ω_L is the locked frequency, N is an integer, $\delta n < 1$ and ϕ is the desired optical phase difference. The interference described by Eq. (2.1) is valid for values of t_d up to approximately the width of the optical pulses. However, the geometric broadening of the monochromator allows the electric field interference to be detected even though the pulses incident on the monochromator do not temporally overlap.

Figure 2 shows the effect of the monochromator in facilitating interference measurements for delay times larger than the pulse width. Figure 2(a) shows the one-beam-only intensity spectrum. Figure 2(a) also shows the oscillatory fringe pattern which is measured with lock-in detection when two pulses with the separations shown in Fig. 2(b) are incident on the entrance slit. The spectral resolution of the monochromator used for the measurements of Fig. 2 was 0.04 nm.

Operationally, two-pulse phase locking is obtained in the following manner. A sinusoidal signal from a function generator is fed to the PZT driver to induce small-amplitude modulation ($\approx \lambda/10$) of the length of the PZT arm of the interferometer, hence in the relative distance traveled by the two pulses. The same sinusoidal signal is used as the reference input to the PLL lock-in amplifier. When the pulses are temporally separated by times less than the Fourier transform of the spectral resolution of the monochromator ($t_d < 30$ or 45 ps) the electric field interference is modulated at the same frequency. The measured signal reflects the net phase of the two-pulse interference for the selected bandpass. The lock-in monitors the first derivative of the light intensity I transmitted by the monochromator

$$\frac{dI}{dl} = -2\pi I_0 \sin \Gamma, \tag{2.3}$$

and compares this quantity to the phase of the reference signal to derive the appropriate error signal (both in sign and magnitude) for feedback to the PZT.

The PLL feedback stability condition for in-phase and out-of-phase pulses is

$$\frac{dI}{dl} = 0, \tag{2.4}$$

and is satisfied when the accumulated phase Γ is equal to $2\pi l/\lambda = M\pi$, for integer M. The sign of the signal indicates whether the time delay is closer to the previous or to the next

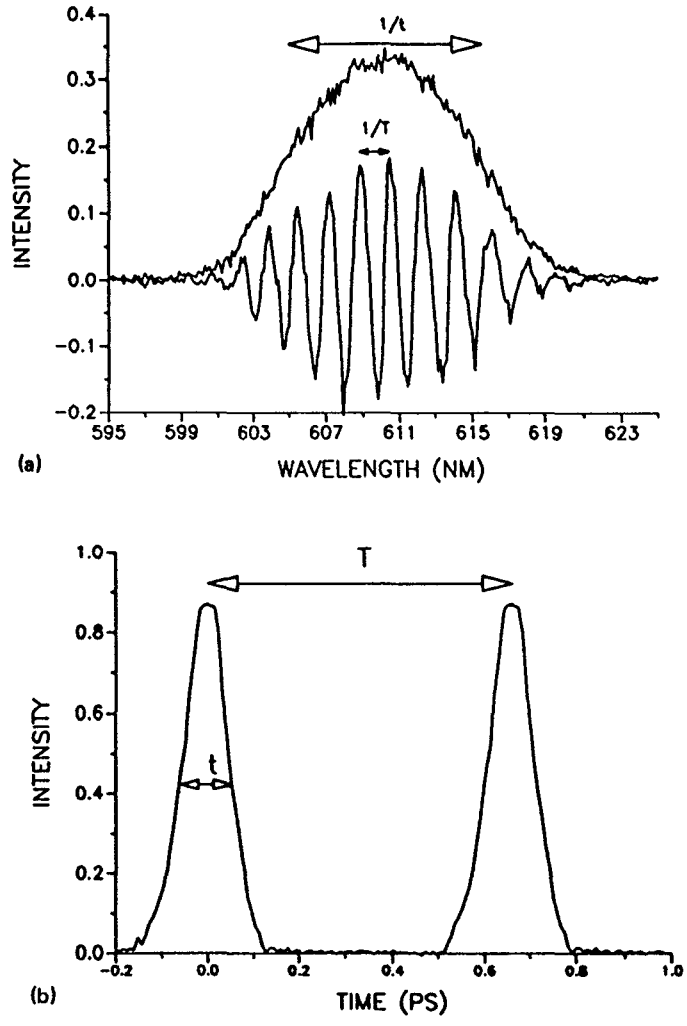

FIG. 2. (a) Intensity spectrum of a single laser pulse and two-pulse spectrum. (b) Intensity autocorrelations of two laser pulses separated by time T and of width t.

integral multiple (for $\phi = 0$) or integral plus one half multiple (for $\phi = \pi$) of a period of the locked wavelength λ. The output of the lock-in amplifier is used as an error signal to adjust the position of the PZT to maintain the desired phase difference, i.e., to make $\delta n = 0$. The quasi-dc output from the lock-in amplifier is added, via a differential amplifier, to the sinusoidal signal going to the PZT driver.

The lock-in amplifier may be adjusted to detect dI/dl or d^2I/dl^2 so that the PLL is capable of maintaining the relative phases of the optical pulses equal to 0 or π thus satisfying Eq. (2.4), or to $\pi/2$ when measuring d^2I/dl^2. The corrections to the position of the PZT are made following each step of the optical delay line. The gain of the lock-in feedback signal is adjusted so that the PZT undergoes excursions of magnitude less than one wavelength of light at any fixed position of the delay line.

The overall frequency response to the PLL is limited to frequencies that are fivefold smaller than the mechanical chopper frequency. This restriction follows from the requirement that the PLL lock-in amplifier produce an error signal which is referenced only to the phase modulation of

This article is copyrighted as indicated in the article. Reuse of AIP content is subject to the terms at: http://scitation.aip.org/termsconditions. Downloaded to IP: 128.32.208.2 On: Thu, 29 May 2014 17:58:57

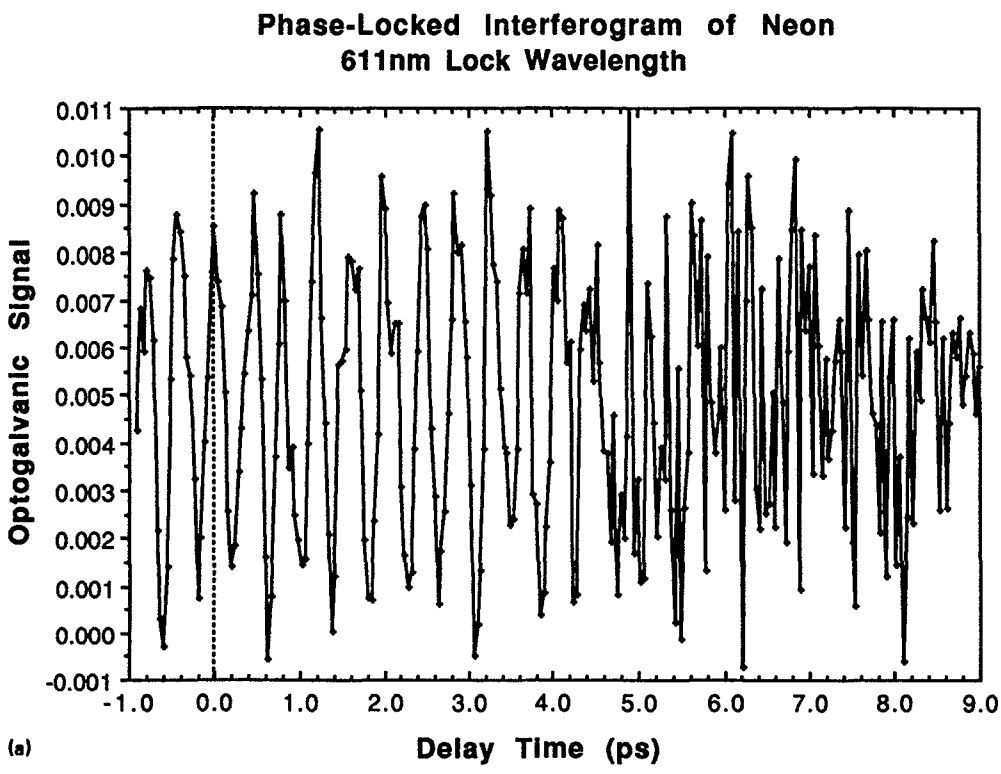

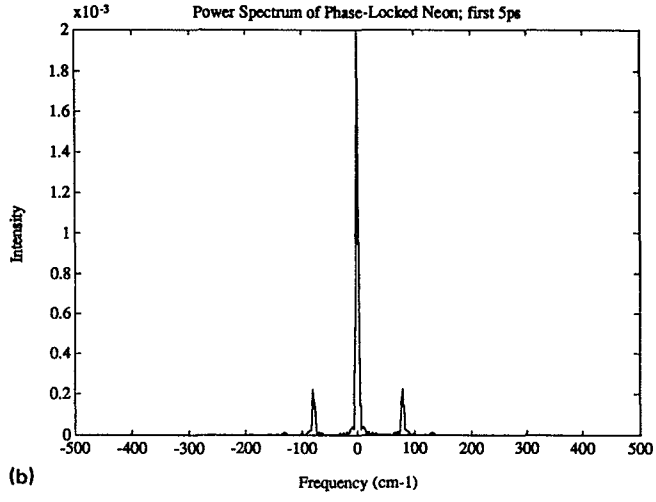

FIG. 3. (a) Phase-locked interferogram of Ne in hollow cathode lamp discharge. Signal recorded for single frequency amplitude modulation thereby detecting the two-pulse interference signal and the two one-beam-only signals. (b) Power spectrum of 0–5 ps delay portion of (a), obtained via Fourier transform.

the PZT and not to sources of amplitude modulation. Furthermore, the frequency response must be smaller than the frequency at which the translation stage sweeps through many wavelengths of delay per stepped advance. This implies that the PLL only responds to correct the relative phase error of the pulse pair after the scanning delay line has come to rest. The PLL bandwidth is about 10 Hz, which is adequate to correct for the low frequency motions of the optical table and mirror mounts and the thermal drift of the interferometer. The PLL stability is relatively insensitive to amplitude fluctuations in the dye laser beam.

C. Phase-locked interferogram of a two level system

Since we can generate short pulses with center wavelength in the range from 608 to 613 nm and large spectral width ($\approx$10–12 nm FWHM), it is possible to excite the 614.3 and 616.4 nm transitions of Ne.[21] This simple system was used to evaluate the performance of the phase-locked pulse pair apparatus. The required metastable initial states were prepared in an Fe hollow cathode lamp discharge, and the optically induced population change monitored via the optogalvanic effect. In the case of these two optical transitions the excited levels are more easily ionized by subsequent collisions with the electrons in the discharge. Therefore, the discharge current will increase for greater excited state population. Figure 3(a) displays the optogalvanic signal as a function of time delay for pulse time delays of less than 9 ps for a locked wavelength of 611.2 nm. The oscillatory transient seen in this figure is symmetric about $t = 0$ and has a period of about 400 fs. We call the reader's attention to the

This article is copyrighted as indicated in the article. Reuse of AIP content is subject to the terms at: http://scitation.aip.org/termsconditions. Downloaded to IP: 128.32.208.2 On: Thu, 29 May 2014 17:58:57

discontinuous change in oscillatory behavior at 4.75 ps. In this particular case, the PLL could not track the relative phase of the pulses for time delays greater than 4.75 ps. At this time delay, for the spectral bandpass and PLL gain used, the PLL can no longer distinguish between in-phase and out-of-phase pulse pairs. This occurs at a time delay less than the transform of the monochromator spectral resolution and results from the insufficient gain in the feedback loop. It will be shown below that phase locking can be obtained for delay times greater than 20 ps.

The modulation of the phase-locked pump–probe measurement for in-phase pulse pairs shows a maximum in the signal level when $t = 0$. The signal detection scheme employed here involves only single frequency amplitude modulation of both beams; therefore, zero signal level corresponds to no laser induced population in the excited levels. A positive signal implies the existence of a greater population in the excited states. The signal approaches zero for time delays of about $\pm$ 200 fs, indicating that the combined effect of the pump and probe pulses with this delay is to return the system to the initial (metastable) states. Figure 3(b) shows the deconvoluted power spectrum of the first 5 ps range of Fig. 3(a). The zero frequency feature arises from the single frequency amplitude modulation scheme; i.e., this form of amplitude modulation results in a dc offset. The 80 and 130 cm^{-1} features correspond to frequency differences between the locked frequency and the two transition frequencies.

The phase of the atomic system following the first pulse evolves[22] as $\exp[i\epsilon_{12}t]$, while the phase of the optical pulses is maintained such that $\phi = 0$ at frequency Ω_L. Thus a beat frequency is expected at $\epsilon_{12} - \Omega_L$, as is observed; in a multilevel system we expect each of the frequency differences $\epsilon_{if} - \Omega_L$ to contribute to the time dependence of the observed signal. The subscripts 1 and 2 refer to the initial and final levels, as do subscripts i and f.

III. EXPERIMENTAL RESULTS

A. Phase-locked transients for molecular iodine

We have chosen I_2 as the vehicle with which to demonstrate molecular spectroscopy with phase-locked pulse pairs. In particular, we report the measurement of the fluorescence-detected interferogram for the $X \rightarrow B$ transition of isolated I_2 molecules.[23]

The idea of the experiment as performed on a single molecule is illustrated in Fig. 4. The first pulse, at zero delay ($t = 0$), prepares a rovibrational wave packet on the B state potential energy surface.[24] This wave packet, which is nonstationary under the Hamiltonian for the B state, undergoes oscillatory motion along the bond coordinate with period $2\pi/\omega_B$, where ω_B is the average vibrational frequency for the superposed vibrational excitations constituting the wave packet. The probe pulse, delayed by t_d, has the same intensity as the pump pulse, and it excites a second wave packet on the B state potential energy curve. The presence of both fields yields a fluorescence signal with contributions proportional to E_1^2, $2E_1E_2$, and E_2^2. The double amplitude-modulation detection scheme described above measures only the E_1E_2 cross term which is proportional to the overlap of the two wave packets. If the initially prepared wave packet has

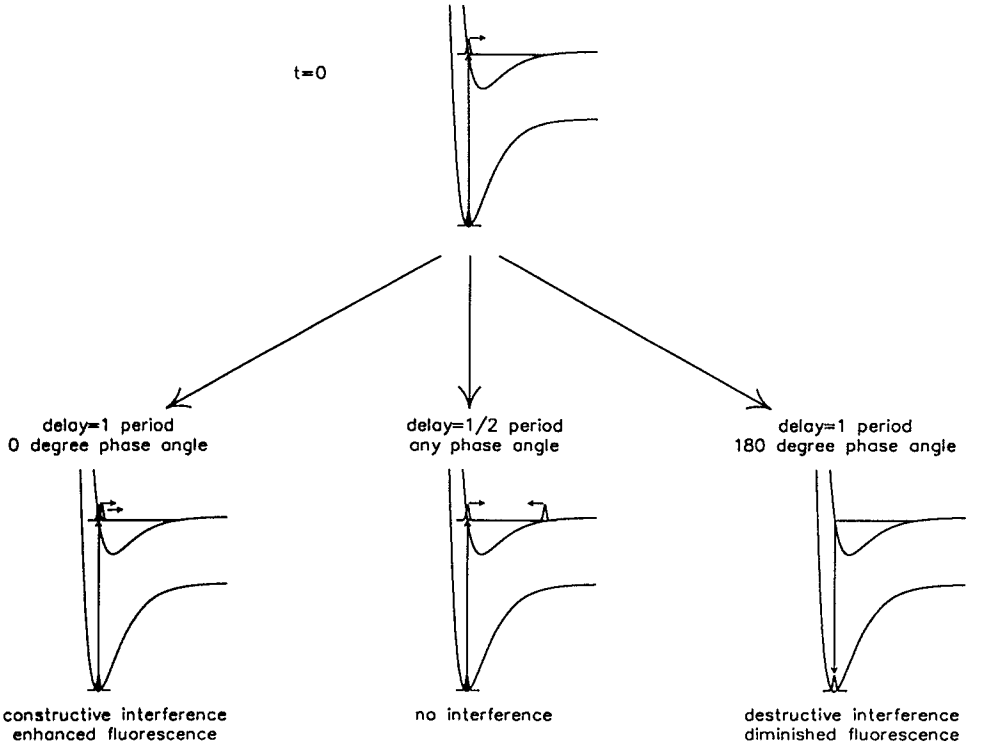

FIG. 4. Schematic illustration of wave packet interferometry applied to molecular systems. First pulse prepares excited state amplitude, the subsequent second pulse can cause constructive or destructive interference for relative phase angles of 0 or 180. There is no interference for delay times that are not integral multiples of the vibrational period of the excited state. This figure refers to a homogeneous system. In actual systems the observed behavior will result from a superposition of responses from the inhomogeneous ensemble.

This article is copyrighted as indicated in the article. Reuse of AIP content is subject to the terms at: http://scitation.aip.org/termsconditions. Downloaded to IP: 128.32.208.2 On: Thu, 29 May 2014 17:58:57

not returned to the Franck–Condon region of the potential energy curves at the time of arrival of the delayed pulse, the interference of the two wave packets will vanish. However, if the delayed pulse arrives near any time satisfying $t = 2\pi n/\omega_B$, net constructive or destructive interference can occur. The response of an ensemble of molecules in an inhomogeneous environment or distribution of initial states will tend to reduce the efficiency of the modulation of the excited state population.

The short pulses used in the experiments have considerable spectral breadth. Only the relative phases of the locked frequency Fourier components of the pulses are fixed, but the near transform limited character of the pulses provides knowledge of the phases of all of the frequency components of the delayed pulse and hence of all the eigenfunction components of the second wave packet at any time delay.

A typical transient response of molecular I_2 is shown in Fig. 5. The measured quantity is the time integrated component of the fluorescence from the B state which depends on the interference of the two excitations. Figure 5(a) displays the data obtained when the pulse pair is locked in-phase ($\phi = 0$). The transient fluorescence signal is referenced to zero by virtue of the double amplitude modulation and detection scheme described earlier. A positive signal thus implies that the excited state population has been increased, with respect to the two one-beam-only contributions to the population, by wave packet interference. A negative signal indicates that the excited state population has been decreased by wave packet interference.

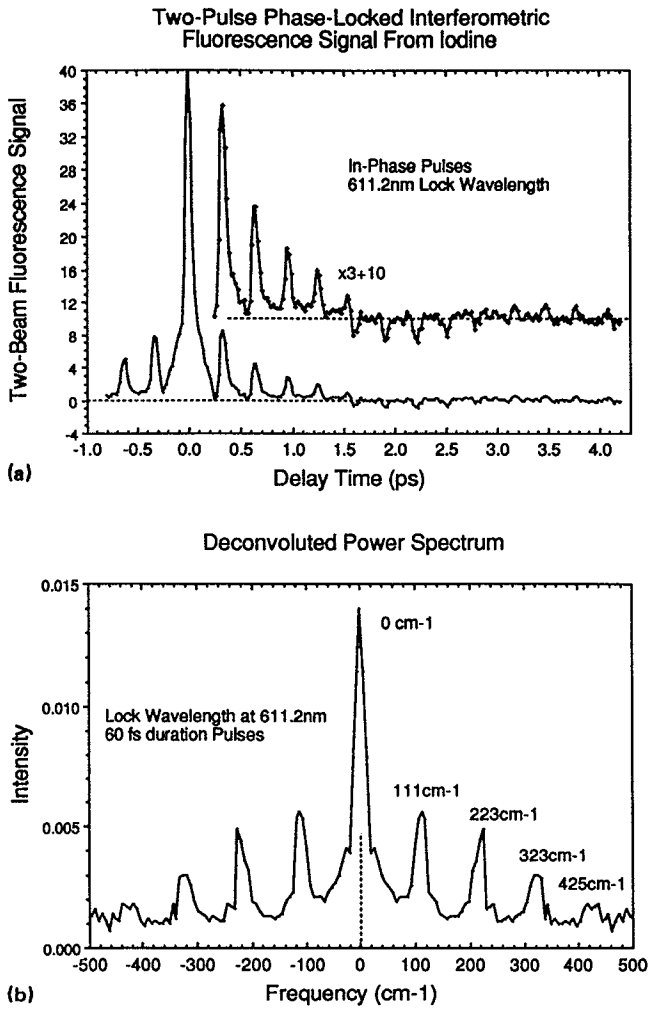

FIG. 5. (a) In-phase fluorescence detected interferogram. Inset shows expanded view of recurrence features. (b) Deconvoluted power spectrum of (a). Deconvolution in Fourier space with Fourier transform of associated phase-locked electric field autocorrelation function. Asymmetric laser pulse spectrum (Ref. 35).

The data displayed in Fig. 5(a), and enlarged in the inset, show a sequence of prominent spikelike features with a 300 fs spacing. The recurrence spacing corresponds to the period of the superposition vibrational levels of the B state which are pumped by optical excitation at 611.2 nm from the thermally populated levels of the ground state. Net constructive or destructive interference of the two wave packets prepared by the pump and delayed probe pulses only occurs at or near multiples of the vibrational period, hence the spikes reflect the return of the coherent vibrational wave packet to the Franck–Condon region. The excited state population will be either enhanced or diminished according to whether the overall phase and de Broglie factors of the overlapping wave packets prepared by the initial and delayed pulses cause them to interfere constructively or destructively, respectively. The overall reduction of the recurrence intensity with increasing pulse delay is a consequence of the phase evolution of the initially prepared superposition of rotational levels in the wave packet (see Sec. V).[25] The wave form is in contrast to the simple "two-level" dynamics observed in Fig. 3 for Ne.

The relative amplitude of the recurrence features does not depend on the beam size in the sample cell. Unfocused beams (of diam 1.5 mm vs 0.1 mm focused) give the same interferogram and recurrence amplitudes as those displayed above. Furthermore, the signal level has a linear dependence on the total light intensity on the sample. These observations are additional indications that the signal is first order in the field of each beam.

Another interesting aspect of the data displayed in Fig. 5(a) is seen near the fifth and sixth vibrational recurrences: the sign of the amplitude of the recurrence changes from positive to negative. This result implies that the phase of the initial wave packet has evolved from in-phase to out-of-phase with the reference wave packet prepared by the delayed pulse. The sign of the recurrence amplitude reverses again after ten periods, as may be seen in the enlarged inset. The phase reversals are accompanied by a shift in the regular 300 fs period of the recurrences. In particular, the separation of the positive to negative signal for the fifth and sixth recurrences is about 450 fs, or 1.5 periods.

It will be shown in Sec. IV that an inverted region can occur when the locked frequency does not resonantly connect each thermally occupied initial vibronic level with *some* excited state vibrational level. This is in keeping with a ubiquitous occurrence of an inverted region in iodine at room temperature, given the thermal occupation of several ground

This article is copyrighted as indicated in the article. Reuse of AIP content is subject to the terms at: http://scitation.aip.org/termsconditions. Downloaded to IP: 128.32.208.2 On: Thu, 29 May 2014 17:58:57

state levels and the disparity between ground and excited state vibrational frequencies.

Figure 5(b) shows the deconvoluted power spectrum of Fig. 5(a). The observed progression of peaks occurs with a 111 cm^{-1} spacing which extends to more than four quanta. The frequency and progression is characteristic of the *B*-state vibrational frequency. The width of each spike in the spectrum is larger than the approximately 4 cm^{-1} resolution expected from the data sampled only over a 4 ps time interval. The excess width arises from the contributions of the rotational states associated with each vibrational state in the composition of the wave packet. Deconvolution with the experimental response function gives the proper weighting of the difference frequency features in the spectrum. The response function used for deconvolution was the measured in-phase phase-locked electric field interferometric autocorrelation function.[16]

It is illustrative to compare the phase-locked results with those obtained from interferometric scans of the pump–probe delay without phase locking. Figure 6(a) shows a composite of the in-phase and out-of-phase signals for a locked wavelength of 611.2 nm, while Fig. 6(b) shows the data points of the not-phase-locked interferometric scan. The two curves in Fig. 6(a) are mirror images of each other; the reflection symmetry is about zero signal level. Clearly, the phase-locked interferograms with phase angles of 0 and π follow the maxima and minima of the not-phase-locked interferometric data for delay times somewhat less than five vibrational periods. The double-lobed feature at the fifth recurrence in Fig. 6(a), not reflected in Fig. 6(b), corresponds to a region in the phase-locked interferogram where the sign of the first wave packet changes from being in-phase (out of phase) to being out-of-phase (in-phase) with the second wave packet for phase-locking angle 0 (π). The envelope of the "free-phase" interferogram is sensitive to the magnitude of the spatial overlap between the wave packets but not to their relative phase. The form of the free-phase interferogram is not influenced by the choice of a locked frequency; rather it is dictated by (i) the molecular absorption spectrum, (ii) the spectral profile of the pulses, (iii) the carrier frequency detuning from resonance with the molecular transitions, and (iv) the sampling frequency (i.e., point density).

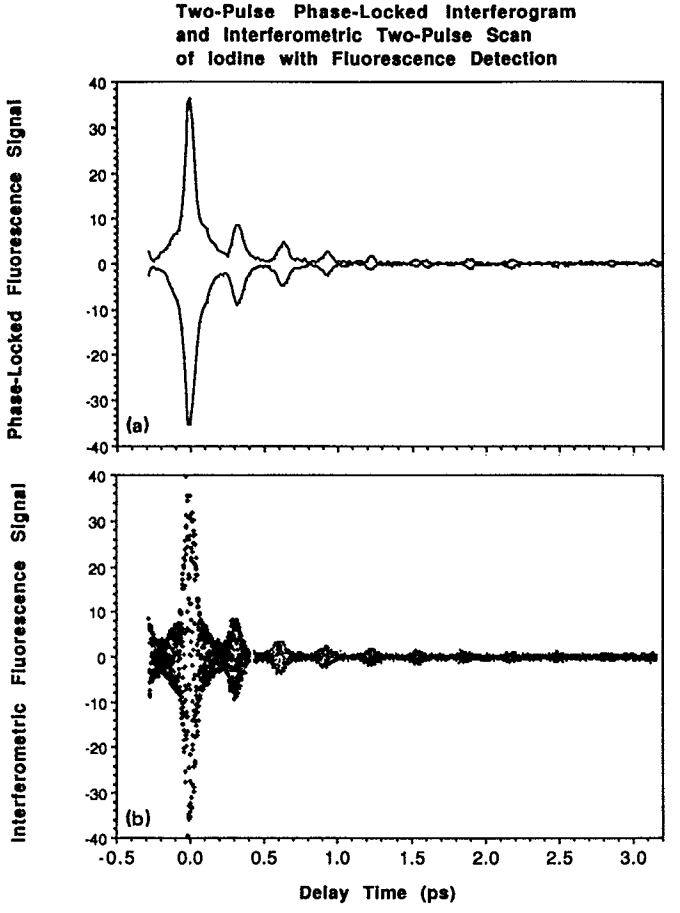

FIG. 6. (a) In-phase and out-of-phase fluorescence detected interferograms with 611.2 nm locked and 611 nm carrier wavelength. (b) Not-phase-locked interferogram for the same pulse duration and spectrum as (a). Time steps are 16 fs for (a) and 0.67 fs for (b).

The Nyquist criterion requires that a sinusoidal signal be sampled at least twice per cycle in order that its apparent frequency, after discrete Fourier transformation, be its true frequency. If this is not the case the apparent frequency will be aliased into a low frequency range. The Nyquist criterion for the data shown in Fig. 6(b) is, when expressed as a sampling period, 0.67 fs, while that for the data shown in Fig. 6(a) is 16 fs. By collecting data only at time delays that are integral multiples (or integral multiples plus one-half) of the optical period corresponding to the locked frequency, we are systematically undersampling the interferometric transient. The phase-locking technique thereby shifts the optical frequencies of Fig. 6(b) to the lower frequencies of Fig. 6(a). That undersampling can be used to obtain high resolution spectra with a reduced data set has been demonstrated in a number of Fourier transform spectroscopies, e.g., optical emission[26] and mass spectrometry.[27]

B. Locked frequency detuning studies

Figure 7 shows a series of in-phase fluorescence detected interferograms for different detunings of the locked wavelength from the molecular resonances[28] or prominent features in the absorption spectrum. The carrier wavelength of the pulses is maintained at approximately 611 nm. Figure 7(a) shows data for a locked wavelength of 611.2 nm. The very regular and symmetric shape of the recurrence features reflects the symmetric pulse spectrum. Further discussion of the effect of the pulse spectrum on the transient wave form will be discussed elsewhere. The interferogram in Fig. 7(a) again has become inverted at the fifth recurrence, near 1.6 ps delay. Figure 7(b) shows the wave form obtained when the locked wavelength is set to 611.5 nm. The inversion occurs at the third recurrence at 0.95 ps delay. Figure 7(c) is obtained when the locked wavelength is set to 611.9 nm and the inversion occurs between the first and second recurrences. Moreover, Fig. 7(c) shows a negative amplitude feature between the $t = 0$ spike and the first recurrence. This negative signal level arises, in part, from the detuning of the pulse carrier

This article is copyrighted as indicated in the article. Reuse of AIP content is subject to the terms at: http://scitation.aip.org/termsconditions. Downloaded to IP: 128.32.208.2 On: Thu, 29 May 2014 17:58:57

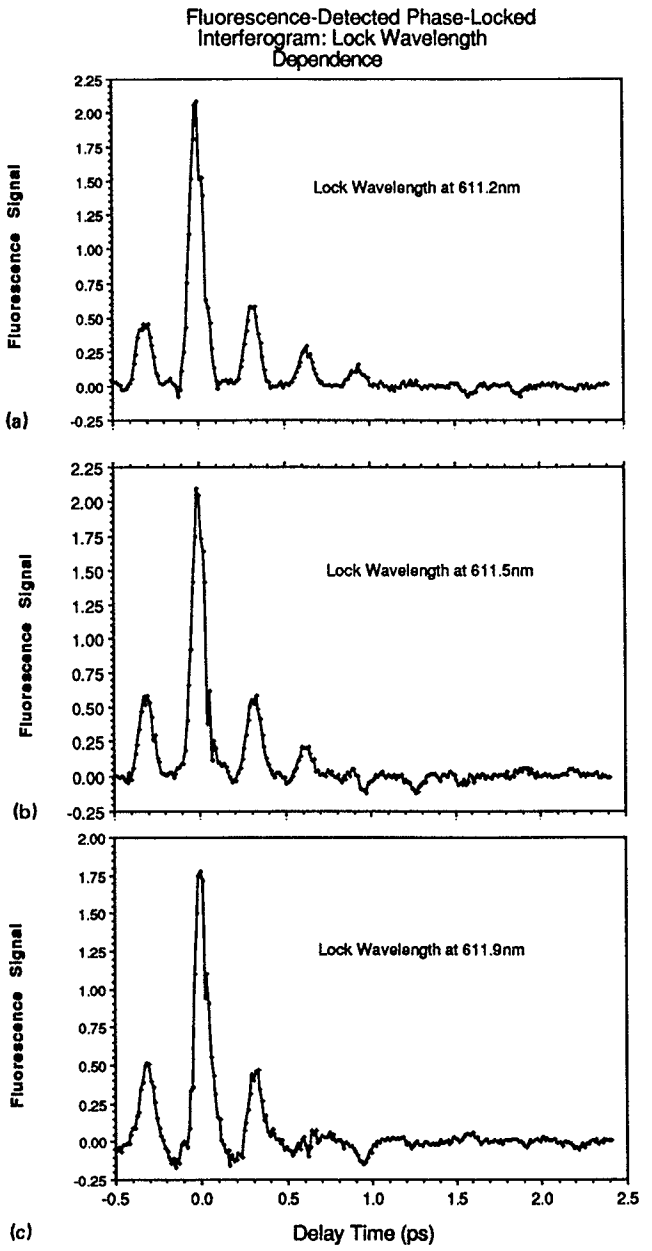

FIG. 7. Dependence of in-phase interferogram on locked wavelength with 611 nm carrier wavelength. (a) 611.2 nm locked wavelength. (b) 611.5 nm locked wavelength. (c) 611.9 nm locked wavelength. Nearly symmetric pulse spectrum (Ref. 35).

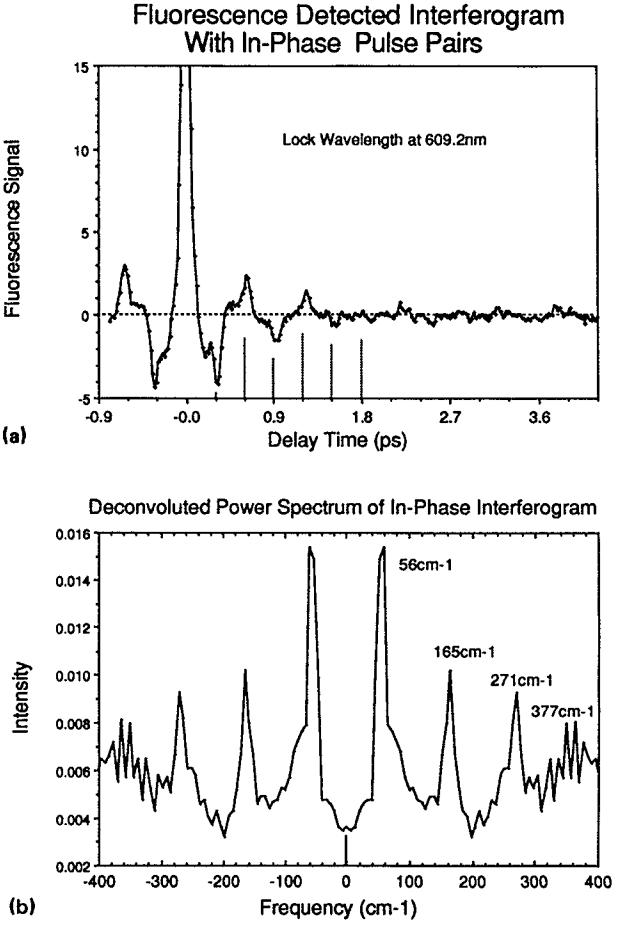

FIG. 8. Maximally detuned in-phase interferogram. (a) 609.2 nm locked wavelength, 610 nm carrier wavelength. (b) Power spectrum of (a), deconvoluted with in-phase electric field autocorrelation for locked and carrier wavelengths in (a).

frequency from the locked frequency. It will be shown elsewhere[16] that the phase-locked electric field autocorrelations have similar sign modulation features about the $t = 0$ delay when the locked and carrier frequencies are not equivalent. Deconvolution with the pulse-locked electric field autocorrelation function serves to account for the differences between the locked and carrier frequency provided that the pulse spectrum is well represented as a symmeric Gaussian. The final point to note is that the second phase inversion, as seen in Fig. 5 and Fig. 7, shifts from about 3.2 [not shown in Fig. 7(a)] to 1.9 to 1.6 ps delay as the locked wavelength is changed to larger values.

The locked wavelength in Figs. 5(a) and 7(a) is the same to within the 0.1 nm precision of setting the monochromator. This imprecision contributes to the difference in appearance of these interferograms. See Sec. V for other considerations (e.g., rotations, pulse spectrum).

Figure 8(a) shows that if the locked wavelength is tuned to 609.2 nm the interferogram waveform is dominated by a prompt negative feature at 300 fs and recurrence features of alternating sign every 300 fs. This is a maximally resonance detuned condition. It can be concluded that tuning the locked wavelength has the effect of altering the location of the recurrence amplitude inversion, and thereby also the overall appearance of the transient fluorescence interferogram. Figure 8(b) shows the deconvoluted power spectrum of Fig. 8(a). In contrast to Fig. 5(b), the present power spectrum does not have a zero frequency feature. Actually, the first spectral features occur at 56 cm^{-1}, which is half of the excited state vibrational level spacing. This figure shows that the dynamics measured by two-pulse phase-locked spectroscopy are directly dependent on the transition energies of the states that constitute the wave packet. The $t = 0$ feature in Fig. 8(a) is approximately seven times the magni-

This article is copyrighted as indicated in the article. Reuse of AIP content is subject to the terms at: http://scitation.aip.org/termsconditions. Downloaded to IP: 128.32.208.2 On: Thu, 29 May 2014 17:58:57

tude of the first recurrence and has been cut off in these and some of the following figures to allow for greater clarity in presenting the modulated behavior away from $t_d = 0$.

IV. THEORETICAL ANALYSIS OF THE FLUORESCENCE INTERFEROGRAM

The experiments described in the preceding sections clearly establish that control of the phases of the pulses in a two-pulse sequence can be used to affect the efficiency of generating the final state of the system and the nature of the final state. This version of phase-locked spectroscopy is related to, but not identical with, the Tannor–Rice[2,3] scheme for enhancing the formation of a selected product in a reaction. It differs from that scheme in that the present experiment is designed to control the total population on the excited state surface by superposing amplitudes rather than to control the population of a product formed in one region on the ground state surface; it resembles that scheme in emphasizing the role of time delay between pulses to control transition probability.

In this section we develop a theoretical analysis which explains the several features of the observations reported in the experimental portion of this paper. We begin with the analysis of a sample harmonic oscillator system for which analytic results can be obtained, and then report the results for numerical calculations for the I_2 system.

We focus attention on the following observations:

(1) Peaks in the transient fluorescence signal appear at regular intervals with respect to the delay between the pulses.

(2) The sign of the amplitude of the transient fluorescence peaks and their form can be altered by changing the phase locking angle. We remind the reader that the intensity of the transient fluorescence due to the interaction of the phase-locked pulse pair with the molecule is referenced to the fluorescence signal in the absence of interference effects (which, by virtue of the double modulation used in the experiments, contributes nothing to the signal), so that positive and negative peaks in the response correspond to increased or decreased intensity, respectively, resulting from interference effects.

(3) For a given phase-locking angle the sign of the transient fluorescence peaks changes after some (typically long) time delay between pulses.

(4) The periodic modulation of the transient fluorescence shows an overall decay with a time constant of roughly 500 fs even though the fluorescence lifetime of I_2 is much longer (>100 ns at room temperature number densities).

(5) The form of the transient fluorescence interferogram is more sensitive to changes in the phase-locked frequency than to changes in the carrier frequency.

The qualitative interpretation of each of these observations has been described earlier; a more quantitative interpretation follows.

A. Fluorescence interferogram of a model diatomic molecule

We first undertake an analysis of the fluorescence interferogram to be expected from the simplest model of an isolated diatomic molecule with two bound electronic states. In this model the potential energy curves corresponding to the nuclear displacements in the two electronic states are taken to be harmonic and to have the same frequencies but displaced origins (see Fig. 9). Rotational motion of the molecule is ignored. The Hamiltonian then has the simple form

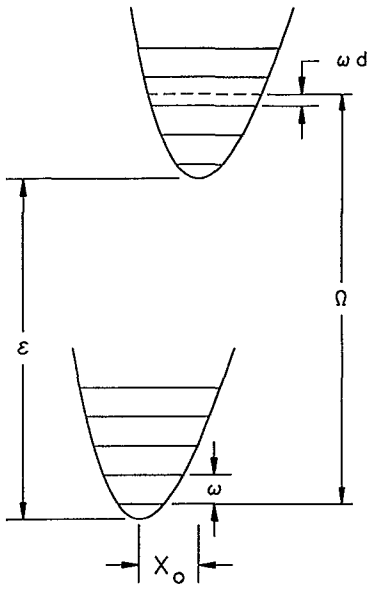

FIG. 9. Potential energy curves for the harmonic oscillator model. Ω is the locked laser frequency, ϵ is the bare transition frequency, ω is the vibrational frequency, X_0 is the equilibrium offset between ground and excited electronic states, and ωd is the resonance offset.

$$H = |g\rangle H_g \langle g| + |e\rangle H_e \langle e|, \tag{4.1}$$

where

$$H_g = (P^2/2M) + (M\omega^2/2)(X + X_0)^2 \tag{4.2}$$

and

$$H_e = \epsilon + (P^2/2M) + (M\omega^2/2)X^2 \tag{4.3}$$

are the ground and excited state nuclear Hamiltonians, respectively. As usual, M, ω, P, and X are the mass, frequency, momentum, and displacement of the harmonic oscillators whose minima differ in energy by ϵ and in equilibrium separation by X_0. The ground and excited electronic eigenstates, $|g\rangle$ and $|e\rangle$, are assumed to have zero static dipole moments. The dipole moment operator then has the form

$$\mu = \mu_{eg}(|e\rangle\langle g| + |g\rangle\langle e|), \tag{4.4}$$

and the interaction with the laser field is

$$V(t) = -\mu E(t). \tag{4.5}$$

We now suppose the model diatomic molecule system is driven by a laser field consisting of two very short Gaussian pulses which are separated in time. It is further assumed that there is a definite phase relationship between the two pulses (to be specified below). The overall time dependence of the laser field is then

$$E(t) = E_1(t) + E_2(t), \tag{4.6}$$

where

This article is copyrighted as indicated in the article. Reuse of AIP content is subject to the terms at: http://scitation.aip.org/termsconditions. Downloaded to IP: 128.32.208.2 On: Thu, 29 May 2014 17:58:57

$$E_1(t) = E_0 \exp[-t^2/2\tau^2]\cos(\Omega t) \tag{4.7}$$

and

$$E_2 = E_0 \exp[-(t-t_d)^2/2\tau^2]\cos(\Omega t + \phi). \tag{4.8}$$

The frequency Ω is chosen to be close to that corresponding to the electronic energy difference between the two surfaces, while the angle ϕ specifies the relative phase of the center frequency (i.e., locked frequency) components of the two pulses. For simplicity we treat the case that the response of the system to the applied field is vibrationally abrupt, which requires that the very short pulses satisfy the condition $(2\pi/\omega) \gg \tau \gg (2\pi/\Omega)$. In fact, for the experiments reported earlier in this paper the pulse widths were not a completely negligible fraction of the typical vibrational periods of the levels excited in I_2. This matter will be dealt with in Sec. IV B.

We assume that the initial state of the system is the lowest ($v'' = 0$) vibrational level of the electronic ground state, and that it is excited to a linear combination of vibrational levels of the upper electronic state by the resonant laser pump pulse. In the experiments described earlier the I_2 sample was at room temperature, so the initial state of the system had a thermal distribution of population in the vibrational levels of the ground electronic state. The numerical analysis described in the next section shows that the aggregate fluorescence signal emitted from upper state levels which were pumped from the levels with $v'' > 0$ has greater intensity than that originating from $v'' = 0$, but has qualitatively similar time dependence.

With these assumptions we recognize that the state of the molecule after the application of a pulse-delayed pulse pair can be represented by

$$|\Psi(t)\rangle = U_{t-t_d-\delta} W_2 U_{t_d-2\delta} W_1 U_{-\delta} |g\rangle|0_g\rangle, \tag{4.9}$$

i.e., the state of the molecule at time t is determined by the combination of driven evolution with the field on and free evolution in the intervals when the field is off. The periods of free evolution are governed by the free molecule Hamiltonian (4.1), so that

$$U_t = \exp[-iHt], \tag{4.10}$$

while during the two intervals of duration 2δ, somewhat greater than 2τ, the time development is, to first order in the field,

$$W_j = U_\delta (1 + iF_j) U_\delta, \tag{4.11}$$

$$F_j = \int_{t_j-\delta}^{t_j+\delta} dt'\, U_{t_j-t'} \mu E_j(t') U_{t'-t_j}; \quad t_2 = t_d, \quad t_1 = 0, \tag{4.12}$$

which expressions are obtained from the first order in E_0 expansion of the propagators in the interaction representation transformed back to the Schrödinger representation. Using Eqs. (4.11) and (4.12) we can rewrite Eq. (4.9) in the form

$$|\Psi(t)\rangle = (U_t + iU_{t-t_d} F_2 U_{t_d} + iU_t F_1)|g\rangle|0_g\rangle, \tag{4.13}$$

which shows, as expected, that the probability amplitude for the system to be found in the excited electronic state is a sum of two terms:

$$\langle e|\Psi(t)\rangle = i \exp[-iH_e(t-t_d)]\{\langle e|F_2|g\rangle \times \exp[-i\omega t_d/2] + \exp[-iH_e t_d]\langle e|F_1|g\rangle\}|0_g\rangle. \tag{4.14}$$

The wave packet prepared on the upper potential energy surface by the initial pulse develops for a time t_d under the nuclear Hamiltonian H_e. The delayed pulse then superposes with this wave packet a second wave packet which has undergone only (stationary) evolution under the ground state nuclear Hamiltonian H_g. We are clearly dealing with the analog of a two slit experiment in which the excited state amplitude can be prepared by two routes not distinguished by experiment.

Using the impulse approximation, which amounts to neglecting nuclear motion during the two pulses and is valid when $\omega\delta$ and $(\epsilon - \Omega)^2\tau^2$ are both much smaller than unity, we find that

$$\langle e|F_j|g\rangle \cong \int_{t_j-\delta}^{t_j+\delta} dt' \exp[i(H_e - H_g) \times (t' - t_j)]\mu_{eg} E_j(t') = \int_{-\infty}^{\infty} dt' \exp[i\epsilon(t' - t_j)]\mu_{eg} E_j(t'). \tag{4.15}$$

Writing $E_j(t')$ as a sum of exponentials and rejecting the off-resonace term (the rotating wave approximation) then yields

$$\langle e|F_1|g\rangle = \mu_{eg} E_0 \tau (\pi/2)^{1/2} \equiv F,$$
$$\langle e|F_2|g\rangle = F \exp[-i(\Omega t_d + \phi)]. \tag{4.16}$$

Substitution of Eq. (4.16) in Eq. (4.14) simplifies the expression for the excited state amplitude. Immediately after the delayed pulse the excited state amplitude can be written in the form

$$\langle e|\Psi(t_d)\rangle = iF\{\exp[-i\{(\Omega + \omega/2)t_d + \phi\}] + \exp[-iH_e t_d]\}|0_g\rangle. \tag{4.17}$$

Note that the phase change of the laser field determines the phase of the wave packet generated by the delayed pulse.

The observed fluorescence signal is determined by the excited state population, which is given by

$$P(t_d) = \langle \Psi(t_d)|e\rangle\langle e|\Psi(t_d)\rangle = F^2\{2 + 2\,\mathrm{Re}[\exp(i((\Omega + \omega/2)t_d + \phi)) \times \langle 0_g|\exp[-iH_e t_d]|0_g\rangle]\}. \tag{4.18}$$

The first term inside the curly brackets of Eq. (4.18) is the excited state population arising from the independent actions of the two pulses; it has this form in the linear approximation because (i) the two pulses are taken to have the same central frequency, shape, and duration, (ii) the depletion of population of the ground state by the pump pulse is very small, so (iii) the delayed pulse adds excitation amplitude to the upper state. The possibility of interference between the wave packets excited by the initial and the delayed pulses is described by the second term inside the curly brackets of Eq. (4.18); from its form we anticipate that the fluorescence signal for a given pulse delay time will be strongly dependent

This article is copyrighted as indicated in the article. Reuse of AIP content is subject to the terms at: http://scitation.aip.org/termsconditions. Downloaded to IP: 128.32.208.2 On: Thu, 29 May 2014 17:58:57

on both the phase locking angle ϕ and the center frequency Ω of the laser pulses. The extent of the interference also depends on the overlap of the initial Gaussian $|0_g\rangle$ with itself after moving for a time t_d on the excited state potential energy curve. This overlap function is of the same type as appears in the time integral expression for the continuous absorption spectrum.[29] The interference contribution to the excited state population corresponds to what has been measured experimentally, as reported in the earlier sections of this paper.

We shall see that the carrier frequency dependent exponential in Eq. (4.18) tends to nearly cancel a large and uninteresting phase in the overlap function which arises from the electronic excitation energy. Because of this near cancellation, the portion of the overlap kernel representing the nuclear dynamics, including the contribution to the wave packet phase from the nuclear motion, will be manifested directly as a function of time.

The nature of the information provided in an experiment of the kind described here is clarified by the form of Eq. (4.18). That expression implies that the real and the imaginary parts of the overlap function can be obtained separately by using two values of the phase locking angle differing by $\pi/2$. The imaginary part of the overlap function is proportional to the time dependent dipole susceptibility for this simple system. By isolating the imaginary part of the overlap function with an appropriate combination of in-phase and in-quadrature data one can directly obtain the dipole susceptibility $\chi(t_d)$.[30] This will be discussed in detail in another paper.

Consideration of some of the detailed characteristics of wave packet propagation in the model system sheds light on the intramolecular processes that will influence the predicted fluorescence signal. The vibrational state $|0_g\rangle = \exp[iPX_0]|0_e\rangle$ is a displaced harmonic oscillator ground state function on the upper state potential energy curve. After propagation for a time t (we now drop the subscript) this wave packet takes the form[31]

$$\begin{aligned}\langle X|\exp[-iH_e t]|0_g\rangle &= (\pi\Delta^2)^{-1/4}\exp[iP_t(X-X_t)] \\ &\times\exp[-(X-X_t)^2/2\Delta^2]\exp[i\gamma_t],\end{aligned} \tag{4.19}$$

where

$$\begin{aligned}P_t &= M\omega X_0 \sin\omega t, \\ X_t &= -X_0\cos\omega t, \\ \gamma_t &= -(X_0^2/4\Delta^2)\sin 2\omega t - [\epsilon + (\omega/2)]t, \\ \Delta &= (M\omega)^{-1/2}.\end{aligned} \tag{4.20}$$

The overlap of Eq. (4.19) with $\langle 0_g|X\rangle$ can be calculated by integrating over X to obtain[32]

$$\begin{aligned}\langle 0_g|\exp[-iH_e t]|0_g\rangle &= \exp[-(X_t+X_0)^2/4\Delta^2]\exp[-\Delta^2P_t^2/4] \\ &\times\exp[-iP_t(X_t+X_0)/2]\exp[i\gamma_t],\end{aligned} \tag{4.21}$$

so the interference term in the excited state population (4.18) is proportional to

$$\begin{aligned}&2\exp[-(X_t+X_0)^2/4\Delta^2-\Delta^2P_t^2/4] \\ &\quad\times\cos[(\Omega+\omega/2)t+\phi+\gamma_t-P_t(X_t+X_0)/2] \\ &= 2\exp[-(Q^2/2)(1-\cos\omega t)] \\ &\quad\times\cos[(\Omega-\epsilon)t+\phi-(Q^2/2)\sin\omega t],\end{aligned} \tag{4.22}$$

where $Q\equiv X_0/\Delta$ is the dimensionless displacement of the origins of the two potential energy curves. The exponential factor in Eq. (4.22) monitors the spatial and momentum overlap of the moving wave packet with the Franck–Condon region of the potential energy curves. Note that the cosine term in Eq. (4.22) is sensitive to the phase and de Broglie factors acquired during t_d by the propagating wave packet, in addition to the laser frequency and the phase locking angle. As will be discussed further below (and in Appendix A) the argument of the cosine in the interference term also represents the phase difference between the time derivative of the oscillating dipole moment induced by the first pulse and the locked field component of the second (delayed) pulse. The use of this representation leads to an alternative interpretation of the transient fluorescence signal as a measure of the efficiency of interaction between the second pulse and the sample polarization induced by the first pulse.

We are now able to describe the fluorescence interferogram. The overlap exponential in Eq. (4.21) is peaked at multiples of the vibrational period, as shown in Fig. 10(a). The calculations displayed in this figure correspond to choosing the reduced displacment $Q^2/2 = 6.4$, a value somewhat smaller than that for the separation of the origins of the X and B state potential energy curves of I_2, which has the effect of exaggerating the widths of the recurrence peaks. The cosine factor in the interference term is, in general, not periodic; it is displayed in Fig. 10(b) with a particular choice of locked or center frequency. Since interference is impossible unless the two wave packets overlap, we need to evaluate the cosine factor in Eq. (4.22) only near the vibrational recurrences, where

$$\omega t = 2\pi n + \sigma; \quad n = 0,1,2,..., \tag{4.23}$$

with σ a small angle. Near the nth overlap peak the argument of the cosine becomes

$$\begin{aligned}&(v'+d)(2\pi n+\sigma)+\phi-(Q^2/2)\sin(2\pi n+\sigma) \\ &\quad\approx 2\pi nd+\phi-[(Q^2/2)-v'-d]\sigma\end{aligned} \tag{4.24}$$

within an integer multiple of 2π. In Eq. (4.24) we have written the difference between the locked center frequency and the frequency of the zero–zero transition of the model molecule as

$$\Omega-\epsilon = (v'+d)\omega; \quad -(1/2) < d \leqslant (1/2). \tag{4.25}$$

This notation is chosen to emphasize that the locked component frequency is closed to being in resonance with the transition $Xv''=0 \leftrightarrow Bv'$.[33] The parameter d is the resonance offset, expressed as a fraction of the vibrational frequency ω (see Fig. 11). The resonance offset produces a secular drift in the argument (4.24). As a result, although constructive interference between the wave packets predominates for the early recurrences (for $\phi = 0$), there is an inverted region with mostly destructive interference when

This article is copyrighted as indicated in the article. Reuse of AIP content is subject to the terms at: http://scitation.aip.org/termsconditions. Downloaded to IP: 128.32.208.2 On: Thu, 29 May 2014 17:58:57

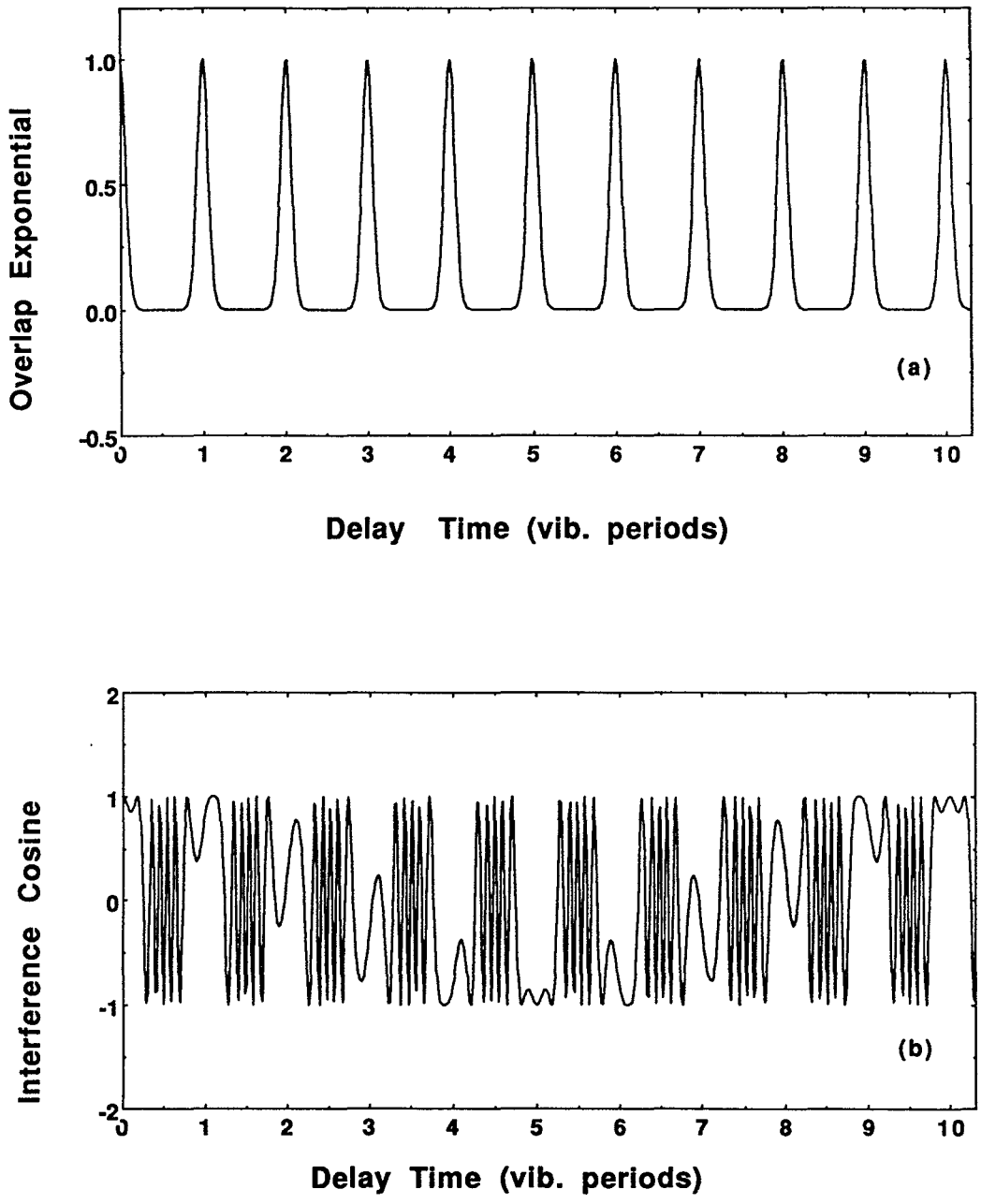

FIG. 10. (a) Plot of the overlap exponential with $Q^2/2 = 6.4$ and $\Omega = \epsilon + 5.1\omega$, illustrating presence of significant overlap only in the Franck–Condon region. (b) Plot of the interference cosine, illustrating how the resonance offset determines the sign at the recurrences.

$$(1/4|d|) \leqslant n \leqslant (3/4|d|). \tag{4.26}$$

Taken together, Eqs. (4.26) and (4.24) show that the location of the inverted region of the fluorescence interferogram is determined by the choice of locked component frequency. On the other hand, the precise positions of the interference maxima and minima depend on the details of the phase development of the first wave packet. These maxima (minima) correspond to regions where the second wave packet increases (decreases) the excited state amplitude.

We restrict our analysis of the phase evolution of the first wave packet to the case when the two laser pulses are in phase, namely $\phi = 0$, and when the resonance offset d is positive. Then for $n \leqslant (1/4d)$, which is prior to the inverted region, the argument of the cosine factor in the interference term is near zero for

$$\sigma = (2\pi n d)[(Q^2/2) - v' - d]^{-1}. \tag{4.27}$$

Equation (4.27) implies that for small pulse delay time the fluorescence maxima will be delayed slightly (i.e., will lag the anticipated times of appearance of recurrences) for Ω less than the vertical transition frequency, since in that case the denominator in Eq. (4.27) is positive. Correspondingly, if Ω is greater than the vertical transition frequency we expect the small pulse delay time fluorescence maxima to occur at times that slightly precede the anticipated recurrence times. Figure 11 illustrates these two cases (for $d = 0.10$). Thus the delay time which produces maximum constructive

This article is copyrighted as indicated in the article. Reuse of AIP content is subject to the terms at: http://scitation.aip.org/termsconditions. Downloaded to IP: 128.32.208.2 On: Thu, 29 May 2014 17:58:57

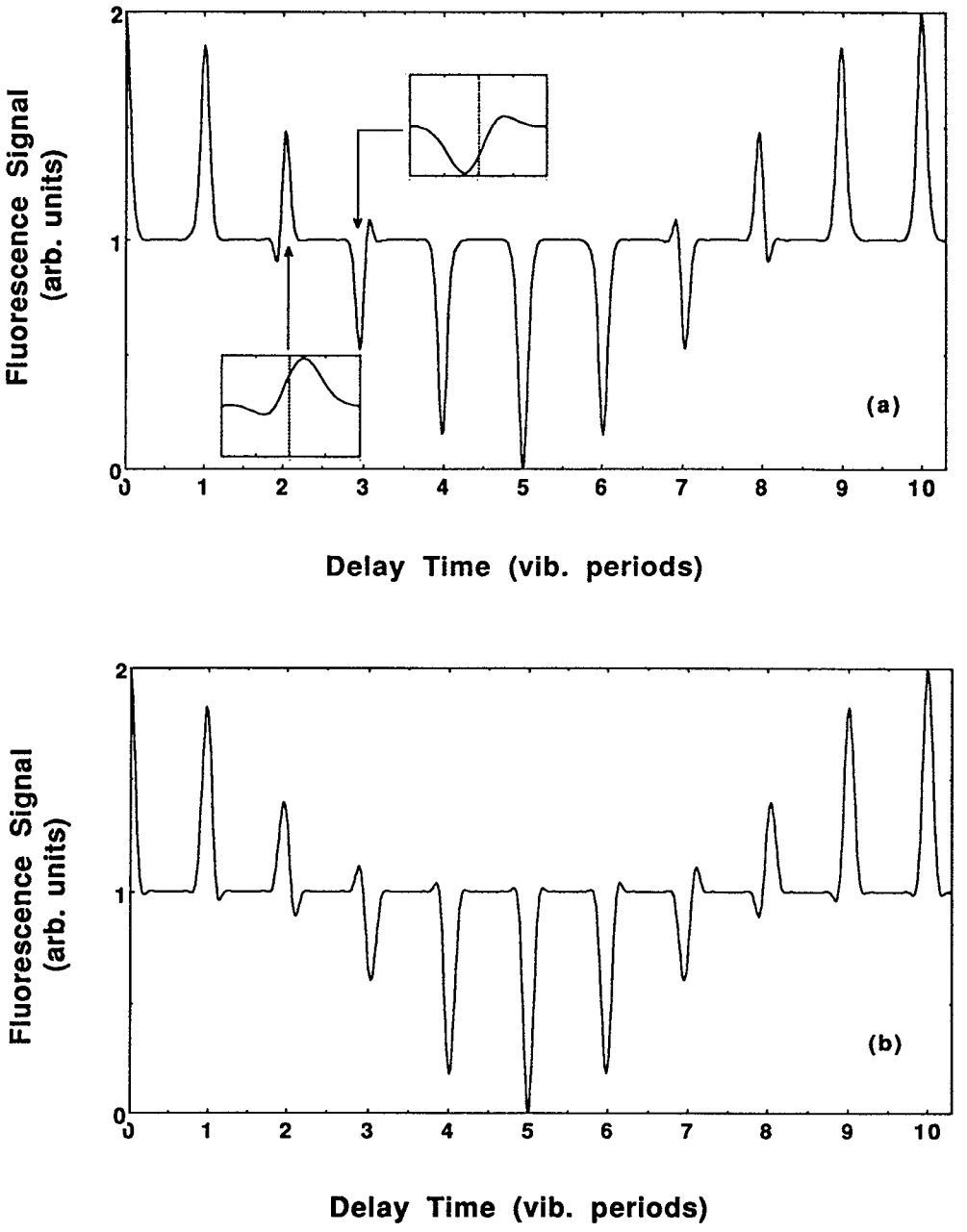

FIG. 11. (a) Fluorescence interferogram with $Q^2/2 = 6.4$ and $\Omega = \epsilon + 5.1\omega$. In this case Ω is below the vertical transition frequency. Plot expansions at the second and third recurrences illustrate fluorescence maxima following and minima preceding the recurrences in the first half of the cycle. (b) Fluorescence interferogram with $Q^2/2 = 6.4$ and $\Omega = \epsilon + 7.1\omega$. In this case Ω is above the vertical transition frequency.

interference represents a compromise between maximum overlap of the propagated wave packet with the Franck–Condon region of the potential energy curves and optimal relative phase of the propagated and reference wave packets.

A similar compromise defines the structure of the vibrational recurrence peaks in the inverted region of the fluorescence interferogram. In this region destructive interference is strongest when

$$\sigma = (2\pi nd - \pi)[(Q^2/2) - v' - d]^{-1}, \qquad (4.28)$$

for which the argument (4.24) of the interference cosine term is π. Thus in the early part of the inverted region and with the center frequency below (above) the vertical transition frequency, destructive interference is most extensive just before (just after) completion of the vibrational cycle. This behavior is evident in Figs. 11. These figures also show that the signs of σ corresponding to maximum destructive and constructive interference, respectively, are reversed beyond the middle of the inverted region.

The discussion thus far has been restricted to the case of positive resonance offset. If the molecular transition frequency closest to the locked laser frequency is greater than Ω, corresponding to $d < 0$, the time shifts for largest constructive and destructive interference change sign from those with $d > 0$. An analysis similar to that given above can be constructed for various cases of pulse pairs in quadrature ($\phi = \pi/2$). Out-of-phase pulses ($\phi = \pi$) are predicted to produce a fluorescence interferogram identical to the corresponding in-phase interferogram except for reflection about the time axis, just as observed.

This article is copyrighted as indicated in the article. Reuse of AIP content is subject to the terms at: http://scitation.aip.org/termsconditions. Downloaded to IP: 128.32.208.2 On: Thu, 29 May 2014 17:58:57

The next section reports quantitative comparisons between the experimental data, many of whose qualitative features have been rationalized here, and the results obtained from a numerical calculations using a more realistic molecular Hamiltonian. In addition, account is taken of the finite spectral width of the laser pulses.

B. Fluorescence interferogram of nonrotating I_2

We now describe two approaches to calculating fluorescence interferograms for I_2. The first approach uses numerical wave packet propagation, and the second approach uses an analytic first order expression that utilizes the known transition frequencies and Franck–Condon overlaps.

1. Numerical wave packet calculations

I_2 differs from the model molecules studied in the last section in several respects, the most important of which for our purposes is that the potential energy curves of the X and B electronic states are anharmonic and support vibrational motions with quite different frequencies. The anharmonicity of the vibrational motion in these states considerably influences both the superposition of levels constituting the wave packets generated by the short laser pulses and the phase evolution of those wave packets which, in turn, affect the fluorescence interferogram. As in the preceding section, we neglect the rotational motion of the I_2 molecule, hence also all aspects of the possible influence of rotation and of vibration–rotation coupling on the fluorescence interferogram. Judged *a posteriori* from the results of the calculations to be presented, the neglect of the effects of molecular rotation on the periodic structure of the fluorescence interferogram is a reasonable approximation. The likely contribution of rotational motion to the initial decay of the fluorescence interferogram was briefly discussed above.

The method of analysis and calculation we have adopted is the same as introduced by Tannor, Kosloff, and Rice.[3] We consider the coupled motion of a molecule with two electronic states, the ground state (g) and an excited state (e), and an applied electric field (E). If the interaction of the molecule with the laser field is accurately represented by Eq. (4.5) for all field strengths the Schrödinger equation for the vibrational motion in this system can be written

$$i\frac{\partial}{\partial t}\begin{bmatrix}\psi_g(t)\\ \psi_e(t)\end{bmatrix} = \begin{bmatrix} H_g(R) & -\mu_{ge}(R)E(t)\\ -\mu_{eg}(R)E(t) & H_e(R)\end{bmatrix}\begin{bmatrix}\psi_g(t)\\ \psi_e(t)\end{bmatrix}, \tag{4.29}$$

where R represents the nuclear coordinates and H_i is the Born–Oppenheimer nuclear Hamiltonian for electronic state i. Equation (4.29) can be solved by numerical integration to give the temporal evolution of the ground and excited state wave functions subjected to any applied field. The computational methods we have used have been described elsewhere;[2,3] some of the computational aspects peculiar to the current application are discussed in Appendix B. In the calculations reported below we have assumed that the electronic transition dipole moment is independent of nuclear displacement (i.e., there is no adiabatic vibronic coupling) and that the envelopes of the laser pulses are Gaussian.

A full mapping of the fluoresence interferogram requires the calculation of the excited state population as a function of delay for two choices of the phase locking angle differing by $\pi/2$. To obtain the needed information we consider the time rate of change of the average excited state population P, which is

$$\frac{\partial}{\partial t}P(t) = \frac{\partial}{\partial t}\langle\psi_e(t)|\psi_e(t)\rangle = \left\langle\psi_e(t)\left|\frac{\partial}{\partial t}\psi_e(t)\right.\right\rangle + \text{c.c.} \tag{4.30}$$

The use of Eq. (4.29) to evaluate the time derivative on the right-hand side of Eq. (4.30) leads to

$$\frac{\partial}{\partial t}P(t) = -2\,\mathrm{Im}[\langle\psi_e(t)|\mu_{eg}|\psi_g(t)\rangle]E(t), \tag{4.31}$$

so that the excited state population change generated by the electric field $E(t)$ is

$$\Delta P = -2\int dt\,\mathrm{Im}[\langle\psi_e(t)|\mu_{eg}|\psi_g(t)\rangle]E(t), \tag{4.32}$$

which shows that the excited state population changes can be associated with the convolution of the electric field with a time dependent transition moment defined by

$$\mu_{ge}(t) \equiv -2\,\mathrm{Im}[\langle\psi_e(t)|\mu_{eg}|\psi_g(t)\rangle]. \tag{4.33}$$

The time dependent transition moment (4.33) can be calculated directly from the numerical wave packet propagation. Of course, if μ_{ge} is independent of internuclear separation the time dependent transition moment is directly proportional to the time dependent overlap. It is shown in Appendix A that Eq. (4.33) is, essentially, the time derivative of the instantaneous molecular dipole moment.

The numerical calculations are further simplified when it is noted that to lowest order in the amplitude of the delayed pulse ψ_e depends only on the field strength of the first laser pulse, while ψ_g is, to lowest order, unaffected by the laser pulses. Thus the change in population induced by the delayed pulse can be efficiently calculated using the following procedure:

(1) Carry out a full nonperturbative wave packet propagation for the ground and excited states using only the amplitude generated by the first pulse. A nonperturbative calculation of the wave packet propagation is not necessary under the weak field conditions appropriate to the experiments we have carried out, but this approach allows us to make use of computer codes already available in this laboratory.

(2) Record the time dependent transition moment defined by Eq. (4.33).

(3) Use Eq. (4.32) for various choices of the electric field of the second pulse to calculate the change in population due to the interaction of the two pulses as a function of pulse delay.

The procedure described has the advantage of avoiding separate wave packet calculations for each choice of delay and phase. Rather, one wave packet propagation is carried

This article is copyrighted as indicated in the article. Reuse of AIP content is subject to the terms at: http://scitation.aip.org/termsconditions. Downloaded to IP: 128.32.208.2 On: Thu, 29 May 2014 17:58:57

out to obtain $\mu_{eg}(t)$, followed by the appropriate convolutions to calculate the population changes.

Notice that we integrate only over the second pulse, so that excited state population generated by the first pulse acting alone is not included. Moreover, population generated by the second pulse acting alone is also omitted from our calculation because the time dependent transition moment is that induced solely by the initial laser pulse. That is to say, we calculate only the interference contribution to the excited state population, precisely the experimentally measured quantity. Since the procedure described neglects the contribution of the second pulse to the time dependent transition moment associated with the first pulse and the resulting change in population, the approach is valid only for pulse separations appreciably larger than the pulse duration. In the simulations discussed in the following text we will omit the short time behavior, corresponding to time delays less than the width of the first recurrence feature, so as to avoid misinterpretation.

Figure 12 shows some typical results of calculations for the I_2 system. The ground state potential energy curve used is taken from the work of LeRoy,[23(a)] and the excited state potential energy curve used is taken from the work of Barrow and Yee.[23(b)] In these calculations it was assumed that the two pulses were transform limited Gaussians with 58 fs FWHM and the same central frequency and intensity. The peak power density was 2×10^{11} W/cm^2. Other calculations we have carried out show that, with the known value of the electronic transition moment for the $X\rightarrow B$ transition ($\mu_{ge}=0.461$ D), the power dependence of the excited state population is linear in the laser intensity at this power density. For this illustration we have taken the phase-locked frequency to be the central frequency of the pulses. And, since I_2 has a rather small vibrational frequency and a substantial thermal population of levels with $v''>0$ in the initial state, Fig. 12 shows the case that the initial state is $v''=3$.

In Fig. 12(a) we show the time dependent transition moment as a function of time for two different choices of center frequency of the pulses. In each case the first laser pulse is centered at $t=0$. For both choices of center frequency the time dependent transition moment shows rapid oscillation at the optical frequencies and a slow amplitude modulation at the vibrational frequency ($\approx$300 fs) due to beating of the coherently excited vibrational levels. In the wave packet picture this beating corresponds to the periodic spatial motion of the excited state wave packet into and out of the Franck–Condon region of the potential energy curves.

Figure 12(b) displays, to lowest order, the excited state population change due to a delayed laser pulse centered at the indicated delay and with a phase-locking angle of zero, calculated using Eq. (4.32) and the time dependent transition moment displayed in Fig. 12(a). Note that the population change retains the periodic modulation at the vibrational frequency, but that the sign of the interference is modulated at a frequency dependent on the choice of laser frequency. The origin of the difference in modulation frequencies emerges from examination of the Fourier transform of the time dependent transition moment, shown in Fig. 12(c). These results should be compared with Figs. 5(b) and 8(b). For both choices of the laser pulse center (locked) frequency there are discrete peaks in the Fourier transforms of the time dependent transition moment, which correspond to resonances with various molecular transitions. When the center wavelength of the pulse is 611 nm the phase-locked frequency is on resonance with at least one molecular transition whereas when the center wavelength of the pulse is 613 nm the phase-locked frequency is detuned from all molecular resonances. The connection between the locked frequency detuning from resonance and the modulation of the sign of the interference signal can be understood in the following way in the context of the present treatment. Of course, the underlying physical process is the same as in the discussion of detuning given in the preceding subsection.

Each frequency component of the time dependent transition moment oscillates in phase with the corresponding frequency component of the first laser pulse. Ignoring vibrational anharmonicity, the components of the quantity (4.33) differ in frequency by the B-state vibrational spacing, and therefore come into phase with each other at the completion of each vibrational period. When the center wavelength of the pulses is 611 nm, the component of the time dependent transition moment at the locked frequency interacts constructively with that field component at all delay times. However, the other contributions to Eq. (4.33) drift in phase relative to their corresponding field components in the delayed pulse. Since the locked frequency is on resonance with a vibronic transition at 611 nm, the drift rates between the transition moment and field components are themselves multiples of the B-state vibrational frequency. Hence phase locking the pulse pair at 611 nm ensures that when the time dependent transition moment refocuses, each contribution to it is in phase with its matching component in the delayed pulse. That is to say, constructive interference takes place at each vibrational recurrence, just as observed in the first panel of Fig. 12(b).

In contrast, when the center wavelength is 613 nm, *all* of the components of the time dependent transition moment drift in phase relative to their matching field components in the delayed pulse. This happens because none of the transition frequencies matches the locked laser frequency, as seen in Fig. 12(c). In this case, the quantity (4.33) still takes on a large amplitude after each vibrational period as the various contributions come into phase with each other. However, the transition moment as a whole is out of phase with the delayed pulse electric field by an amount that changes from recurrence to recurrence at a rate given by the detuning of the locked frequency from the nearest molecular transition. Appendix A treats further the refocusing of the "time dependent transition moment," or dipole derivative and the relative phase of this quantity and the delayed pulse electric field.

Figure 13 displays the results of calculations similar to those that led to the displays in Fig. 12 except that the initial state is taken to be a thermal distribution of initial vibrational states at $T=300$ K. Since each of the states in the initial thermal distribution has a slightly different set of transition frequencies, the detuning of the locked frequency from the nearest resonance differs for each initially occupied level. A

This article is copyrighted as indicated in the article. Reuse of AIP content is subject to the terms at: http://scitation.aip.org/termsconditions. Downloaded to IP: 128.32.208.2 On: Thu, 29 May 2014 17:58:57

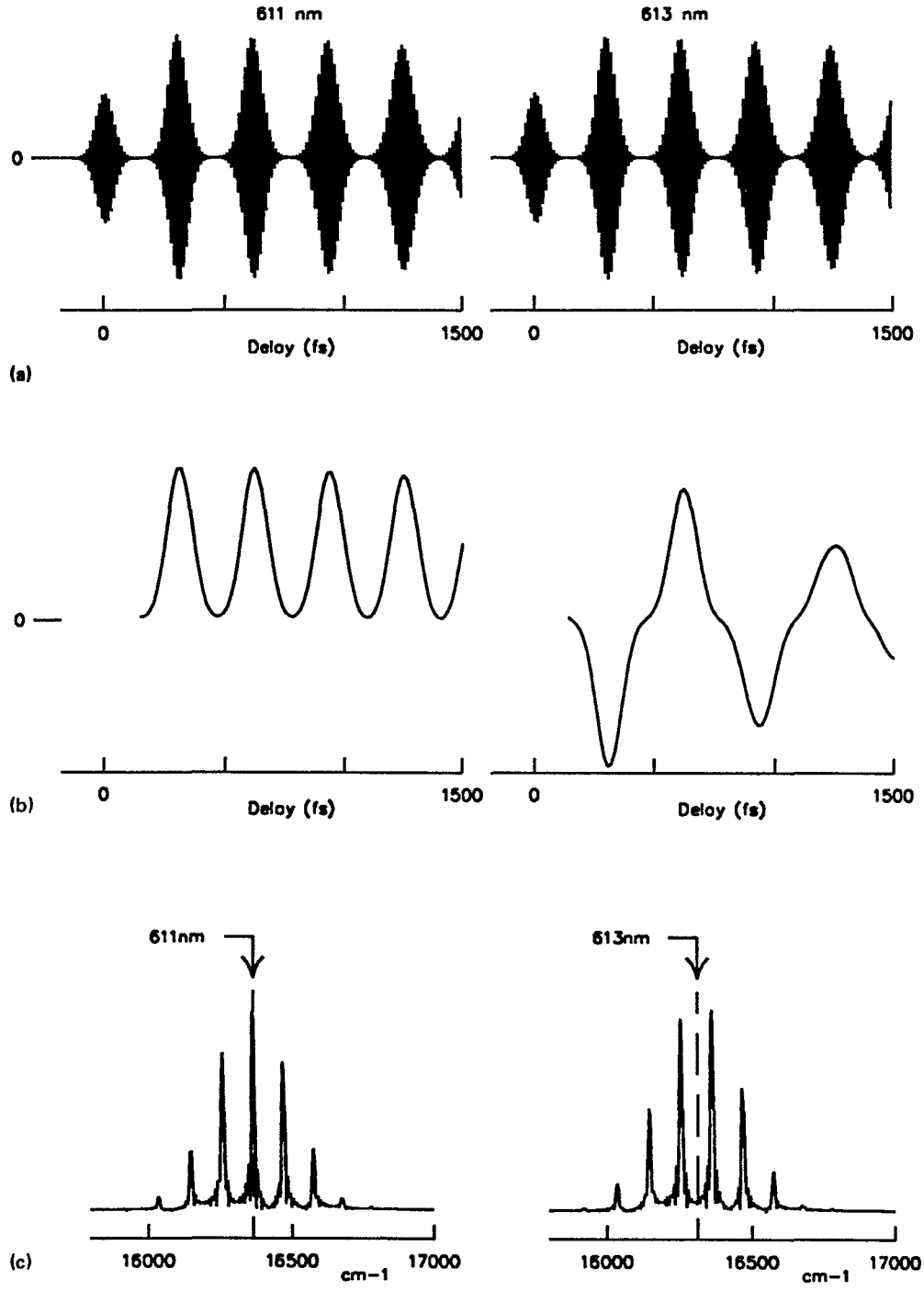

FIG. 12. Numerical wave packet results for the I_2 system for an initial vibrational state of $v'' = 3$ and for two choices of phase locked wavelength (611 and 613 nm). (a) Time dependent transition moment. (b) In-phase interferogram. (b) Fourier spectrum of the time dependent transition moment.

change in sign of the interference with delay time is therefore possible for any choice of locked frequency. The results displayed in Fig. 13 reproduce all the salient feature of the observed fluorescence interferograms obtained with identical locked and carrier frequencies, apart from the overall decay.

In the simulations reported above, the center (carrier) frequency components of the two pulses were assumed to bear a definite phase relationship to each other. That is to say, the carrier frequency components were the ones locked. Phase locking between any component frequencies of the two pulses can be readily incorporated in the numerical wave packet method, but we turn instead to an alternative perturbative treatment to study the effects of detuning the locked frequency from the carrier frequency.

2. Analytic first order calculations

This section describes numerical calculations of the fluorescence interferogram of I_2 using an analytical expression for ΔP^{int} obtained with first order time dependent perturbation theory. Like the numerical wave packet calculations, those described below take into account the width of the

This article is copyrighted as indicated in the article. Reuse of AIP content is subject to the terms at: http://scitation.aip.org/termsconditions. Downloaded to IP: 128.32.208.2 On: Thu, 29 May 2014 17:58:57

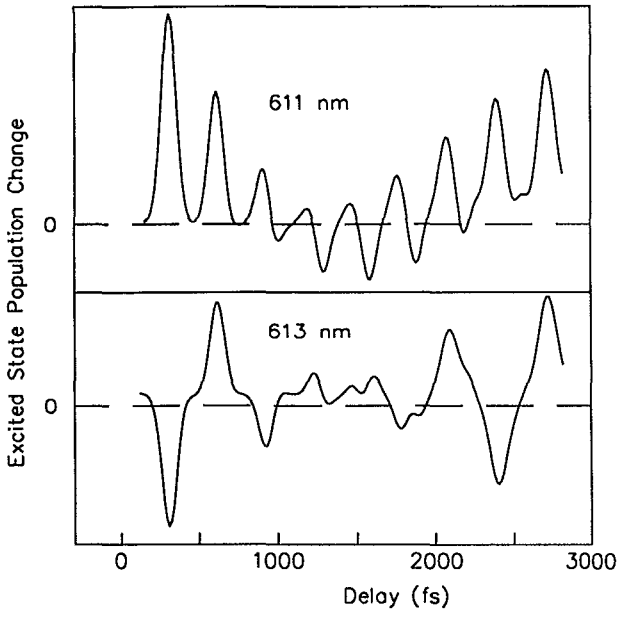

FIG. 13. Numerical wave packet results for the I_2 system with a room temperature distribution of initial vibrational states for two choices of phase locked wavelength (611 and 613 nm).

laser pulses and the anharmonic nature of the potential energy surfaces.

Starting in the vibronic eigenstate $|g\rangle|v''\rangle$, the state of the molecule after its interaction with the pulse pair can be expressed as

$$|\Psi(t)\rangle = \exp(-iHt)\{1 + i\int_{t_0}^{t} dt'[\exp(iHt') \times \mu[E_1(t') + E_2(t')]\exp(-iHt')]\}|g\rangle|v''\rangle, \tag{4.34}$$

where H is given by Eq. (4.1) but with the potentials of H_e and H_g corresponding to the B state and X state of iodine. $E_1(t)$ is given by Eq. (4.7), and $E_2(t)$ takes the form

$$E_2(t) = E_0 \exp[-(t-t_d)^2/2\tau^2] \times \cos[\Omega t + (\Omega_L - \Omega)t_d + \phi)], \tag{4.35}$$

where Ω is the carrier frequency, Ω_L is the locked frequency, ϕ is the phase locking angle, and τ is the pulse width obtained from the experimental FWHM pulse width. It will be shown below that the factor $(\Omega_L - \Omega)t_d$ is necessary in order to lock the pulses with an optical angle ϕ when $\Omega_L \neq \Omega$. From Eq. (4.34) the excited state vibrational wave function prepared by the composite pulse pair can be expressed as

$$\langle e|\Psi(t)\rangle = i\int_{-\infty}^{\infty} dt'\{\exp[-iH_e(t-t')] \times \mu_{eg}[E_1(t') + E_2(t')]\exp(-iH_g t')\}|v''\rangle. \tag{4.36}$$

Insertion of a complete set of vibrational eigenstates of the excited state nuclear Hamiltonian yields

$$\langle e|\Psi(t)\rangle = i\sum_{v'}|v'\rangle\exp(-i\epsilon_{v'}t)\mu_{eg}\langle v'|v''\rangle \times \int_{-\infty}^{\infty} dt'\exp[i(\epsilon_{v'} - \epsilon_{v''})t'] \times [E_1(t') + E_2(t)], \tag{4.37}$$

where the integral is the sum of the Fourier transforms of $E_1(t)$ and $E_2(t)$. Thus Eq. (4.37) can be rewritten as

$$\langle e|\Psi(t)\rangle = i(2\pi)^{1/2}\sum_{v'}|v'\rangle\exp(-\epsilon_{v'}t)\mu_{eg}\langle v'|v''\rangle \times [E_1(\epsilon_{v'} - \epsilon_{v''}) + E_2(\epsilon_{v'} - \epsilon_{v''})], \tag{4.38}$$

with

$$E_1(v) = \frac{E_0\tau}{2}\exp\left[-\frac{\tau^2}{2}(\nu - \Omega)^2\right], \tag{4.39}$$

and

$$E_2(v) = \frac{E_0\tau}{2}\exp\left[-\frac{\tau^2}{2}(\nu - \Omega)^2 \times \exp\{i(\nu - \Omega_L)t_d - i\phi\}\right]. \tag{4.40}$$

Equations (4.39) and (4.40) show that the Fourier components of the pulses at frequency Ω_L satisfy the condition for phase locking with angle ϕ,

$$E_2(\Omega_L) = E_1(\Omega_L)\exp(-i\phi). \tag{4.41}$$

Substituting Eqs. (4.39) and (4.40) into Eq. (4.38) and calculating $|\langle e|\Psi(t)\rangle|^2$ yields the excited state population. The contribution due to interference is given by

$$\Delta P^{\text{int}} = \pi E_0^2\tau^2|\mu_{eg}|^2\sum_{v'}|\langle v'|v''\rangle|^2 \times \exp[-\tau^2(\epsilon_{v'} - \epsilon_{v''} - \Omega)^2] \times \cos[(\epsilon_{v'} - \epsilon_{v''} - \Omega_L)t_d - \phi]. \tag{4.42}$$

From Eq. (4.42) we can see that the contribution to ΔP^{int} from a particular vibronic transition oscillates at a frequency equal to the detuning of that transition from the locked frequency. Its amplitude is determined by the detuning from the carrier frequency and the Franck–Condon factor for the transition.

To calculate the total contribution due to interference, expression (4.42) is evaluated for each thermally accessible v'' and the results are summed with Boltzmann thermal weighting. In these calculations, we use ground state energies from LeRoy,[23(a)] excited state energies from Barrow and Yee,[23(b)] and Franck–Condon overlaps from Tellinghuisen.[23(c)] The laser pulse width used in this calculation is 50 fs FWHM. Expression (4.42) is valid for arbitrary delay and applies without modification to the case of overlapping pulses. For delay times appreciably larger than the pulse width, results obtained by evaluating Eq. (4.42) were found to be identical to those obtained by explicitly propagating the initial wave packet.

We have tested the sensitivity of the signal predicted by Eq. (4.42) to changes in the locked frequency. Figures 14(a)–14(c) show calculated interferograms corresponding to the locked frequency detuning experiments of Figs. 7(a)–

This article is copyrighted as indicated in the article. Reuse of AIP content is subject to the terms at: http://scitation.aip.org/termsconditions. Downloaded to IP: 128.32.208.2 On: Thu, 29 May 2014 17:58:57

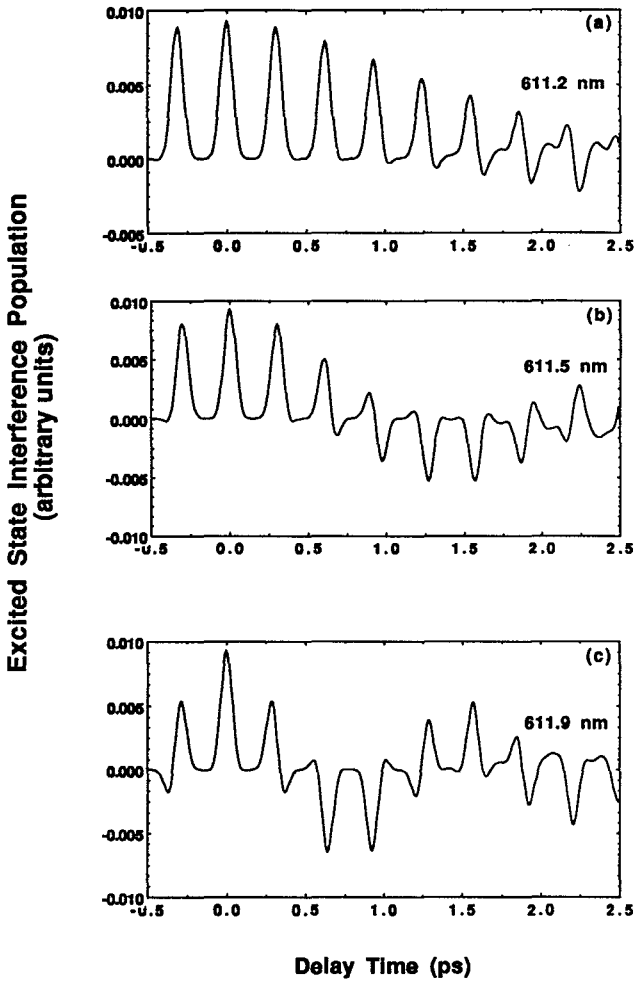

FIG. 14. Theoretical locked wavelength detuning studies with 610.0 nm carrier wavelength. (a) Locked wavelength 611.2 nm. (b) Locked wavelength 611.5 nm. (c) Locked wavelength 611.9 nm. Compare Fig. 7.

7(c). In each case the calculated peak positions are in agreement with their experimental counterparts until the experimental signal has decayed into noise. As the locked wavelength increases, the phase-inversion feature appears at an earlier time delay, as in the experiment. However, the vibrations-only calculations do not correctly predict the exact position of the phase inversion (see Sec. V).

In order to understand the effect of approaching the impulsive limit, where the duration of the laser pulses is a negligible fraction of the vibrational period, we have calculated interferograms for 30 fs pulses (not shown). Significantly more complex recurrence features were obtained for the shorter pulse durations but the pulse duration does not alter the location of the phase inversion. However, at a locked wavelength of 611.2 nm, the delay between the positive portion of the fifth and negative portion of the sixth recurrence features is considerably less than observed in Fig. 5(a).

Figure 15 is a composite of an experimental interferogram and a calculated interferogram obtained using Eq. (4.42). The deviation between experiment and theory near 0.9 ps delay is due to improper tracking of the PLL at this time delay. Much of the essential physics of the process appears to be captured by Eq. (4.42) even though only the vibrational degrees of freedom are included in the calculation. However, the experimental recurrences are somewhat sharper than the calculated features. We attribute this discrepancy to the omission of rotational degrees of freedom from the calculated interferogram (see below).

V. DISCUSSION

A. Comparison of theory and experiment

The previous sections have reported experimental observations, and a theoretical analysis, of the wave forms obtained in phase-locked pulse pair spectroscopy. We now discuss the range of the agreement between the experimental results and the theoretical analysis. The disagreements indicate the limits of validity of the theoretical models and the consequences of nonideal experimental parameters.

The regular spacing of the peaks observed in the interferometric fluorescence signal is obtained in the theoretical studies; the periodicity of the recurrences arises from the partial refocusing of the initially prepared wave packet in the Franck–Condon region of the B-state potential energy surface. The period of the recurrence agrees with the inverse of the vibrational level spacing in the optically accessed region of the excited electronic state, namely about 300–320 fs. The signal levels of the observed features reflect the magnitude of the constructive interference of the coherent superposition states prepared by the two pulses. The short delay time behavior is reminiscent of that predicted numerically by Metiu and Engel in the two-pulse photodissociation yield of NaI.[12]

Both the experimental [cf. Fig. 5(a)] and the theoretical results show the presence of a phase-inversion point where the recurrence signals obtained for in-phase pulses become negative. It has been observed that the further the locked wavelength is tuned away from a prominent feature in the absorption spectrum the sooner the phase inversion occurs. We have found, however, that the inverted region is a ubiquitous feature which cannot be eliminated by simply adjusting the locked wavelength to be "maximally on resonance." We conclude that the delay time at which this inversion occurs results from three factors: (i) the detuning of the locked wavelength from vibronic transition wavelengths, (ii) the difference in the frequency spacing between the ground and excited state vibrational levels, and (iii) the vibrational anharmonicity of the excited state surface. The complexity is compounded by the fact that many transitions occur from each thermally populated ground state vibrational level.

A discrepancy between the harmonic model of Fig. 11 and experiment is found with respect to the delay separation between the last positive and first negative recurrence peaks,

This article is copyrighted as indicated in the article. Reuse of AIP content is subject to the terms at: http://scitation.aip.org/termsconditions. Downloaded to IP: 128.32.208.2 On: Thu, 29 May 2014 17:58:57

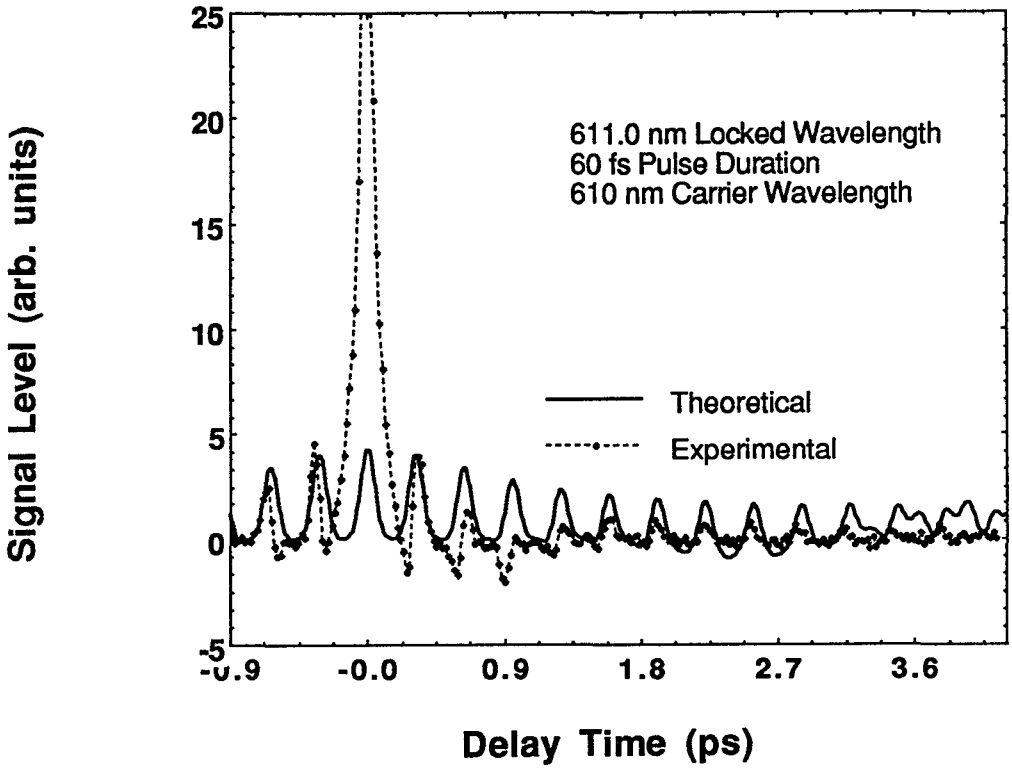

FIG. 15. Comparison of theoretical and calculated in-phase interferograms. The two interferograms were superimposed by matching the amplitude at the first recurrence.

which respectively precede and follow the inversion point. The results from the simple displaced harmonic oscillator model show the phase-inversion feature to be only slightly shifted in time from the 300 fs recurrence period, whereas the experimental results in Fig. 5(a) and Fig. 15 show that the separation is approximately 1.5 periods. The experimental data of Fig. 5(a) and 15 are in much closer agreement with the results of the numerical calculation than with those of the simple displaced harmonic oscillator model (which does not take into account convolution with the nonzero pulse duration). The numerical results of Fig. 15 indicate that the finite duration of the pulses is the main contributing factor to such shifts of the recurrence time in the phase-inversion region. The vibrational anharmonicity of the B state does not play a significant role in determining the shift of the peaks in the inverted region.

The most striking quantitative disagreement between theory and experiment is the time evolution of the amplitude of the recurrence features. The experimental fluorescence interferograms show a rapid initial decay which is not evident in the theoretical results. We attribute this difference to the omission of the rotational degrees of freedom of the molecule from the theoretical analysis. In the real molecular system there are many rovibronic transitions excited by the laser pulse. We then expect that the time development[25] of the superposed rotational levels built on a particular vibrational level will result in a damping of the amplitude of the recurrence features. We note that the amplitude of the first recurrence feature is generally only about 15%–25% of the amplitude of the $t_d = 0$ feature, whereas the subsequent decay of the recurrence amplitude is much more gradual. This behavior contrasts strongly with the behavior of the two-level atomic system (see Fig. 3).

The few picosecond decay of the fluorescence-detected interferogram and shape of the recurrence features, as observed in Figs. 5(a) and 15, is therefore an indication of rotational time development associated with the coherent excitation of many closely spaced rotational sublevels. The decay in the amplitude of the recurrences after the initial fall off from the $t_d = 0$ peak up to the inversion point for the 611.2 nm locked wavelength is not evident in the numerical calculations of Fig. 15. This ensemble time development (also termed dephasing of rotational coherence) occurs in about 2 ps.[34] In the experiments reported the two laser pulses are nearly transform limited, so that in the limiting case that the rotational sublevels form an effective continuum the rotational coherence would decay on the time scale of the laser pulse width. The observation of coherence at longer times via the presence of the recurrences reflects the finite number and limited range of rotational transitions excited, the very small linewidth of each rotational transition, and the finite extent of the rotational band contour associated with each vibrational transition. The time scale for the evolution of an ensemble of rotationally excited molecules can be much greater at low temperature because of fewer thermally populated initial states and the strict rotational selection rules.

We have recently included rotations in the numerical calculations and allowed for the effects of rotation–vibration interaction and centrifugal distortion on the rotational constant. Preliminary calculations indicate that rotations and the spectral shape of the laser pulses play an important role in determining the position of the phase-inversion feature. The results of these calculations will be presented elsewhere[35] and will be used to aid in the interpretation of other locked fequency detuning measurements and dispersed fluorescence measurements not presented here.

This article is copyrighted as indicated in the article. Reuse of AIP content is subject to the terms at: http://scitation.aip.org/termsconditions. Downloaded to IP: 128.32.208.2 On: Thu, 29 May 2014 17:58:57

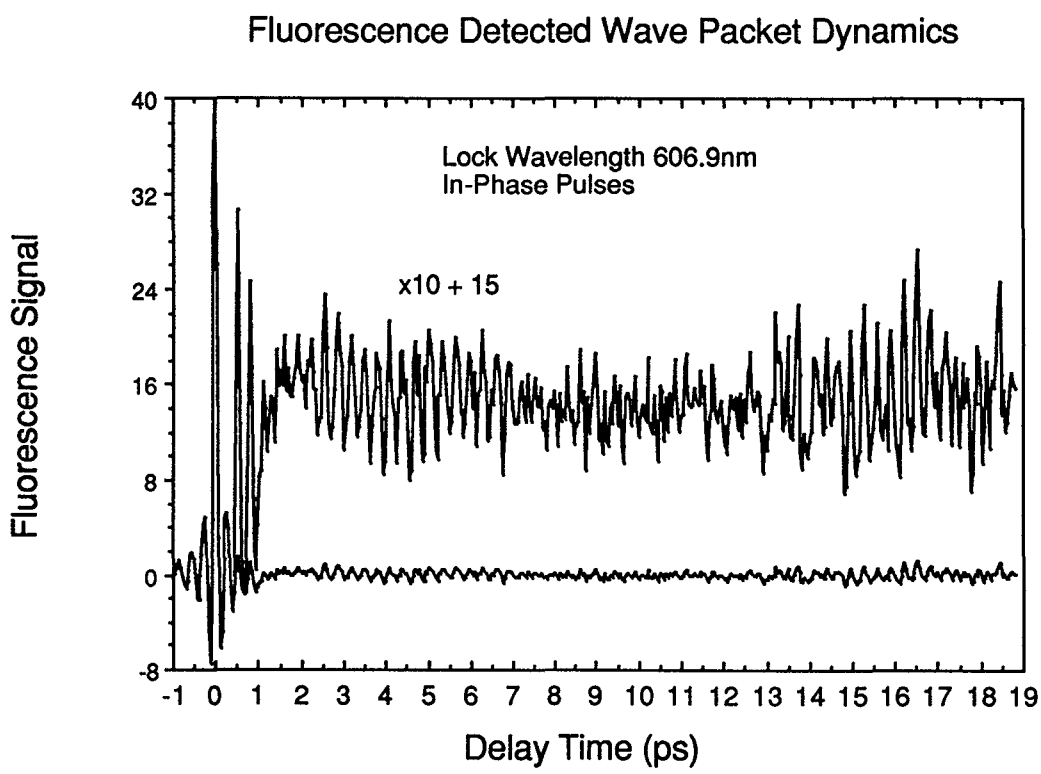

FIG. 16. Long-time phase locking at 606.9 nm locked wavelength and 610–611 nm carrier wavelength with asymmetric pulse spectrum. Inset: Magnified and vertically shifted view of 1–19 ps delay time region.

Will the wave packet reform both spatially and in its phase structure on a still larger time scale? Phase locking for in-phase and out-of-phase pulses could be maintained in excees of 25 ps by increasing the gain of the phase-locked loop. This delay time corresponds to half the transform of the triangular-base resolution of the 0.34 m monochromator with a 1800 g/mm grating. The interference signal level from the PLL PMT has decreased by 30% at 25 ps delay, reflecting the magnitude of the linear dispersion of the monochromator. Figure 16 shows an interferogram for 19 ps total delay for a locked wavelength of 606.9 nm. The well defined oscillatory character of the 300 fs period recurrence features extends for 8 ps and reappears near 14 ps delay. Fourier analysis indicates the presence of spectral features at zero, 110, 220, and 330 cm^{-1}, similar to Fig. 5. The reemergence of the oscillatory envelope at the large time delays occurs with the full amplitude of the pre-8 ps feature. The 8–13 ps delay region corresponds to a highly distorted wave packet, which precludes significant net enhancement or reduction of the signal.

The primary difference between Fig. 16 and Fig. 5 occurs near zero delay time where the in-phase experimental interferogram displays highly oscillatory structure. This behavior, not predicted with Eq. (4.42), is seen in calculations that include rotations.[35] For a locked wavelengths of 611.2 nm, the preliminary calculations are also consistent with experiment, showing no such oscillations. The recurrence features in the fluorescence-detected interferogram persist for a longer period of time for a locked wavelength of 606.9 nm than for locking at 611.2 nm. This can be attributed to the fact that 606.9 nm is close to resonance with two vibronic transitions: $v'' = 2 \rightarrow v' = 10$ and $v'' = 3 \rightarrow v' = 12$. A locked wavelenth of 611.2 nm is close only to the $v'' = 2 \rightarrow v' = 9$ transition.

B. Comparison with other spectroscopies

Spectroscopy with phase-locked pulse pairs, when applied to a two level system, has some features in common with Ramsey fringe spectroscopy.[36] Phase-locked pulse pair interrogation of a two level system will generate an interference pattern that is modulated as a function of delay with frequency $\Omega_L - \omega_{eg}$, with Ω_L the locked frequency. In Ramsey fringe spectroscopy the delay between pulses is fixed and the locked frequency is scanned, which also scans the relative phase of the pulses, whereas in phase-locked pulse pair spectroscopy the phase angle is held fixed while the delay between pulses is varied. In addition, spectroscopy with phase-locked pulse pairs, as applied to a multilevel system, also differs from Ramsey fringe spectroscopy in the use of a spectrally broad pulse, which requires us to account for the various phase angles associated with the different frequency components of the pulse. In practice, the locked frequency need not correspond to the resonant frequency of any one of the possible transitions of the multilevel system. When it does not, the phase angle for the spectral component resonant with a particular transition oscillates as a function of delay time, with a period corresponding to the detuning of the locked frequency from that resonant frequency. The resulting fluorescence interferogram has a complicated structure arising from the different detunings from the several transition frequencies.

This article is copyrighted as indicated in the article. Reuse of AIP content is subject to the terms at: http://scitation.aip.org/termsconditions. Downloaded to IP: 128.32.208.2 On: Thu, 29 May 2014 17:58:57

It is also interesting to compare phase-locked pulse pair spectroscopy with traditional interferometric Fourier transform spectroscopy. The essence of Fourier transform spectroscopy is the conversion of real-time optical fields to an interferometrically recorded low frequency signal, followed by numerical Fourier analysis. This frequency scanning is carried out by an interferometer with a variable delay line. In phase-locked pulse pair spectroscopy a similar frequency demodulation is induced; each frequency component of the time dependent transition moment is converted to a low frequency oscillation. In this sense, phase-locked pulse pair spectroscopy can be thought of as a real time measurement of the optical free induction decay; by shifting to low frequency we have facilitated the probing of the molecular dynamics.[37] There is, also, a difference between these spectroscopies. By virtue of the phase locking, the interference pattern which would be obtained in the absence of phase locking is transformed into a frame of reference which evolves at the locked optical frequency (which is, approximately, the optical carrier frequency). In essence, the full interferogram with frequency components in the optical region may now be undersampled as in the low frequency pattern illustrated in Figs. 6(a) and 12(b). More important, this is accomplished without loss of information about the real and imaginary parts of the first order (linear) susceptibility and the molecular dynamics in the excited state.

VI. CONCLUDING REMARKS

We have presented an experimental demonstration and a theoretical analysis of phase-locked pulse pair spectroscopy. This form of spectroscopy differs from conventional pump–dump (probe) spectroscopy as employed in the experiments of Gerdy *et al.*[11] where the optical phases of the pulses are not controlled, and hence fluctuate rapidly due to mechanical vibrations in the optics and repetitive scanning for signal averaging. Unless the relative optical phases of the pulses are actively controlled, the quantum mechanical interference effects average to zero. The pump–dump method of Ref. 11 is sensitive to the time dependent coordinate distributions of populations generated by the separate pulses and can thereby yield information about excited state population decay, but not about electronic dephasing. Pump–probe measurements performed with disparate frequencies are intrinsically insensitive to electronic dephasing effects due to the lack of a phase relationship of the beams except at $t_d = 0$. Other spectroscopies, such as Raman lineshape and photon echo measurements, exist which monitor electronic dephasing effects.[38]

The special feature about optical spectroscopy with phase-locked pulses is its sensitivity to the phase and de Broglie factors of the wave packet generated by the initial pulse. For instance, intermolecular processes that cause the bare electronic transition energy to fluctuate randomly will increase the decay rate of the interference signal even if these interactions do not sensibly alter the spacing of the excited state vibrational levels. We also anticipate that intramolecular processes contributing to the phase of the wave packet will influence the appearance of the interferogram whether or not these processes affect the wave packet motion. An intramolecular process of this kind, which is absent in I_2, is electronic geometrical phase development,[39(a)] which is predicted to accompany wave packet motion in polyatomic systems in the presence of conical electronic degeneracies between electronic potential energy surfaces. A recent analysis has shown that phase-controlled pulse pairs which resonantly excite transitions between degenerate and nondegenerate electronic levels can explicitly monitor electronic geometrical phase development.[39(b),39(c)]

It will be shown in another paper that Fourier transformation of the in-phase and in-quadrature phase-locked fluorescence interferograms yields the full complex linear susceptibility of the electronic transition. This may be accomplished without Kramers–Kronig transformation. Therefore, a complete determination of the linear susceptibility for transitions within the specified laser bandwidth is possible at optical and ultraviolet wavelengths with reduced sampling (cf. Fig. 6).

Our experimental technique is expected to work better with shorter laser pulses. In numerical calculations, reduction of the pulse duration to 30 fs, which is one tenth of the excited state vibrational period, revealed considerably more detail in the wave packet dynamics. Operationally, the phase locking scheme will work equally well for arbitrarily short duration pulses; in particular, in the limit of a δ-function pulse the concept of an optical carrier frequency is no longer well defined, so that it should be possible to allow for phase locking at arbitrary wavelengths without consideration of the distortions of the wave forms that arise from differences between the carrier and locked wavelengths. Consideration of any phase modulation of the laser pulse will, however, still be important even for pulses of a few femtoseconds duration.

Another important aspect of phase-locked pulse pair spectroscopy is the operational capability to control the optically prepared probability amplitude on an excited state potential energy surface. We have shown that it is possible to enhance or reduce the population of a selected electronic state and the form of the resultant nuclear wave function in that state by the choice of the relative phase of the two pulses, which may be very useful in the further development of recently proposed schemes for the control of molecular dynamics by application of sequences of ultrashort pulses.[2,3]

It is anticipated that the present experimental method can be extended to studies that involve the determination of higher order nonlinear susceptibilities through multiple pulse pump–probe variations of the simple two-pulse scheme described herein. We are especially interested in exploring the possibilities for application to problems of liquid phase dynamics, both pure liquids and solutions, as well as solvation and reaction dynamics in liquids. Preparation of frequency domain gratings in resonant pulsed excitation[40] and manipulation of the induced polarization with selected phase is expected to become a powerful tool in studying the relaxation dynamics in liquids through, for example, free induction decay and three-pulse photon echo probing. Such measurements are currently underway.

This article is copyrighted as indicated in the article. Reuse of AIP content is subject to the terms at: http://scitation.aip.org/termsconditions. Downloaded to IP: 128.32.208.2 On: Thu, 29 May 2014 17:58:57

ACKNOWLEDGMENTS

The research reported in this paper was supported by the National Science Foundation. Helpful conversations with Professor W. S. Warren are gratefully acknowledged. We thank Professor L. D. Zeigler for contributions to the manuscript and tireless assistance in the experimental measurements during the latter stages of this research. N.F.S. acknowledges the National Science Foundation for a postdoctoral fellowship.

APPENDIX A

In this Appendix, we show that the excited state population change produced by the delayed pulse reflects the efficiency with which it couples to the dipole moment induced in the system by the initial laser pulse. The time dependent expectation value of the dipole moment operator is given by

$$\langle \mu(t) \rangle = \int dR \, [\psi_g^*(t), \psi_e^*(t)] \begin{bmatrix} 0 & \mu_{ge} \\ \mu_{eg} & 0 \end{bmatrix} \begin{bmatrix} \Psi_g(t) \\ \Psi_e(t) \end{bmatrix}$$

$$= \langle \psi_g(t) | \mu_{ge} | \psi_e(t) \rangle + \text{c.c.} \tag{A1}$$

The time derivative of the dipole moment is closely related to the quantity (4.33) discussed above. To see this, we differentiate both sides of (A1) and use Eq. (4.29) to obtain

$$\frac{d\langle \mu(t) \rangle}{dt} = 2 \, \text{Im}[\mu_{ge} \langle \psi_g(t) | H_e - H_g | \psi_e(t) \rangle]. \tag{A2}$$

Since vibrational energies are only a few percent of the electronic transition energy, Eq. (A2) can be accurately approximated by

$$\frac{d\langle \mu(t) \rangle}{dt} = 2\epsilon \, \text{Im}[\mu_{ge} \langle \psi_g(t) | \psi_e(t) \rangle], \tag{A3}$$

where ϵ is the bare electronic transition energy. Substitution of Eq. (A3) in Eq. (4.32) leads to an alternative expression for the population change,

$$\Delta P = \frac{1}{\epsilon} \int dt \frac{d\langle \mu(t) \rangle}{dt} E(t)$$

$$= -\frac{1}{\epsilon} \int dt \, \langle \mu(t) \rangle \frac{dE(t)}{dt}, \tag{A4}$$

which has a straightforward physical interpretation. In particular, if we are interested in the interference contribution to the excited state population, then both fields E_1 and E_2 must participate. To lowest order, the dipole moment can to be taken to be that induced by the first pulse alone and the time integration to extend over the second pulse. We then have

$$\Delta P^{\text{int}} = \frac{1}{\epsilon} \int_{t_d - \delta}^{t_d + \delta} dt \frac{d\langle \mu_1(t) \rangle}{dt} E_2(t). \tag{A5}$$

We now briefly consider formula (A5) in application to the model diatomic discussed in Sec. (IV A). For that system, making use of Eqs. (A3), (4.21), (4.20), and (4.16), yields the following expression for the dipole derivative:

$$\frac{d\langle \mu_1(t) \rangle}{dt} = 2\mu_{eg} FRe[e^{i\omega t/2} \langle 0_g | e^{-iH_e t} | 0_g \rangle]$$

$$= 2\mu_{eg} FRe\{e^{-(Q^2/2)(1-\cos \omega t)}$$

$$\times e^{-i[(Q^2/2)\sin \omega t + \epsilon t]}\}. \tag{A6}$$

Using this expression and the form (4.8) for the field, we find that the integrand of Eq. (A5), specifying the rate of population change during the delayed pulse, is given by

$$\frac{d\langle \mu_1(t) \rangle}{dt} E_2(t)$$

$$= \mu_{eg} FE_0 e^{-(t-t_d)^2/2\tau^2} e^{-(Q^2/2)(1-\cos \omega t_d)}$$

$$\times \cos[(\Omega - \epsilon)t_d + \phi - (Q^2/2)\sin \omega t_d]. \tag{A7}$$

The integral of Eq. (A7) over t is the same as the interference term (4.22) obtained previously. But the argument of the cosine in Eq. (A7), an example of which is plotted in Fig. (11b), here represents the phase difference between the oscillating dipole derivative and the locked component of the delayed-pulse electric field. When these two quantities are in-phase (out of phase) the driving field increases (decreases) the energy of the molecule, enlarging (diminishing) the excited state population. When the field and the dipole derivative are $\pi/2$ out of phase the delayed pulse has little effect on the energy of the system. The periodic exponential factor in Eq. (A7) was plotted above in Fig. 11(a). It is now seen to reflect the magnitude of the induced dipole, which is large when the propagated wave packet is in the Franck–Condon region and small when it is not.

APPENDIX B: SOME COMPUTATIONAL DETAILS

The wave packet propagation method we have used is that described by Tannor *et al.*[3]; it involves second order differencing and evaluation of the spatial second derivative by the Fourier method of Kosloff and Kosloff.[3] The wave function is evaluated on a spatial grid with a spacing consistent with the maximum momentum expected during the calculation. As for the time step, previous calculations suggest that it is adequate to take

$$\Delta t < (E_{\max})^{-1}, \tag{B1}$$

where $E_{\max}$ is the maximum energy expected in the calculation. This restriction is, however, not adequate for the analysis of the phase coherent phenomena.

To accurately generate the phase of the wave function over a long time T the temporal frequency of the wave function must be accurate to

$$\Delta\omega \approx T^{-1}. \tag{B2}$$

Kosloff and Kosloff showed that, for a numerical calculation of this type and a system having a constant potential energy V, the wave function temporal frequency ω is related to the discrete wave vector k by

$$\frac{\sin(\omega \Delta t)}{\Delta t} = \frac{1}{m} \sum_{i=1}^{N} k_i^2 + V. \tag{B3}$$

For Δt satisfying Eq. (B1), Eq. (B3) reduces to the expected dispersion relation

This article is copyrighted as indicated in the article. Reuse of AIP content is subject to the terms at: http://scitation.aip.org/termsconditions. Downloaded to IP: 128.32.208.2 On: Thu, 29 May 2014 17:58:57

$$\omega = \frac{1}{m}\sum_{i=1}^{N} k_i^2 + V. \tag{B4}$$

The accuracy of this approximation to lowest order is

$$\Delta\omega = (\omega^3 \Delta t^2)/6, \tag{B5}$$

so that one can expect a phase error of

$$\Delta\phi = (\omega^3 \Delta t^2 T)/6 \tag{B6}$$

over the interval T. Assuming that the population error resulting from a phase error scales as

$$[1 + \cos(\Delta\phi)]/2, \tag{B7}$$

less than 1% error accumulates when

$$\omega^3 \Delta t^2 T < 1.2, \tag{B8}$$

or

$$\omega \Delta t < 1.1(\omega T)^{-1/2}. \tag{B9}$$

Equation (B9) suggests the use of a time step smaller than that given by Eq. (B1) by a factor $(\omega T)^{1/2}$, which is just the square root of the number of optical periods for which the propagation is carried out. This result implies that the accumulated phase error in time T can be interpreted as the sum of random phase errors of magnitude $\omega\Delta t$ for each optical period. Calculations with various values of Δt confirm this interpretation and the validty of the criterion stated in Eq. (B9).

We note that phase error considerations are also important in calculations of wave packet dynamics relevant to experiments with single pulse excitation and in cases not directly involving phase coherence.

[1] P. Brumer and M. Shapiro, Chem. Phys. Lett. **82**, 177 (1986); C. Asaro, P. Brumer, and M. Shapiro, Phys. Rev. Lett. **60**, 1634 (1988); M. Shapiro, J. W. Hepburn, and P. Brumer, Chem. Phys. Lett. **149**, 451 (1988); T. Seideman, M. Shapiro, and P. Brumer, J. Chem. Phys. **90**, 7132 (1989).

[2] D. J. Tannor and S. A. Rice, J. Chem. Phys. **83**, 5013 (1985).

[3] D. J. Tannor, R. Kosloff, and S. A. Rice, J. Chem. Phys. **85**, 5805 (1986). For additional details on the numerical methods employed see D. Kosloff and R. Kosloff, J. Comp. Phys. **52**, 35 (1983).

[4] S. Shi and H. Rabitz, Chem. Phys. **139**, 185 (1989); S. Shi, A. Woody, and H. Rabitz, J. Chem. Phys. **88**, 6870 (1988); **92**, 2927 (1990).

[5] R. Kosloff, S. A. Rice, P. Gaspard, S. Tersigni, and D. J. Tannor, Chem. Phys. **139**, 201 (1989).

[6] A. M. Weiner, J. P. Heritage, and R. N. Thurston, Opt. Lett. **11**, 153 (1986); R. N. Thurston, J. P. Heritage, A. M. Weiner, and W. J. Tomlinson, IEEE J. Quantum Electron. **QE-22**, 682 (1986); A. M. Weiner and J. P. Heritage, Rev. Phys. Appl. **22**, 1619 (1987); A. M. Weiner, D. E. Leaird, G. P. Wiederecht, and K. A. Nelson, Science **247**, 1317 (1990).

[7] (a) F. Spano, M. Haner, and W. S. Warren, Chem. Phys. Lett. **135**, 97 (1987); *Ultrafast Phenomena V*, edited by G. R. Fleming and A. Siegman (Springer, Berlin, 1986), p. 514. (b) Phase and amplitude shaped pulses have also been demonstrated by W. S. Warren and M. S. Silver, Adv. Mag. Reson. **12**, 247 (1988).

[8] N. F. Scherer, A. Ruggiero, M. Du, and G. R. Fleming, J. Chem. Phys. **93**, 856 (1990).

[9] G. F. Thomas, Phys. Rev. A **35**, 5060 (1987).

[10] See, for example, J. J. Yeh and J. H. Eberly, Phys. Rev. A **22**, 1124 (1980); J. Jortner and J. Kommandeur, Chem. Phys. **28**, 273 (1978).

[11] J. J. Gerdy, M. Dantus, R. M. Bowman, and A. H. Zewail, Chem. Phys. Lett. **171**, 1 (1990).

[12] (a) H. Metiu and V. Engel, J. Opt. Soc. Am. B **7**, 1709 (1990); (b) V. Engel and H. Metiu (unpublished work); (c) A. Villaeys and K. F. Freed, Chem. Phys. **13**, 271 (1976).

[13] M. M. Salour, Rev. Mod. Phys. **50**, 667 (1978).

[14] A. Mukherjee, N. Mukherjee, J. C. Diels, and G. Arzumanyan, *Ultrafast Phenomena V* (Springer, Berlin, 1986), p. 166; J. C. Diels and J. Stone, Phys. Rev. A **31**, 2397 (1985); J. C. Diels and S. Besnainou, J. Chem. Phys. **85**, 6347 (1986).

[15] For recent experimental work on phase-related pulses see, J. T. Fourkas, W. L. Wilson, G. Wackerle, A. E. Frost, and M. D. Fayer, J. Opt. Soc. Am. **9**, 1905 (1989).

[16] N. F. Scherer, A. J. Ruggiero, M. Du, H. Guttman, and G. R. Fleming (in preparation).

[17] A. J. Ruggiero, N. F. Scherer, J. N. Hogan, G. M. Mitchel, and G. R. Fleming, J. Opt. Soc. Am. B (in press, 1991).

[18] H. Avramopoulos and R. L. Fork, J. Opt. Soc. Am. B **8**, 117 (1991).

[19] N. H. Schiller and R. R. Alfano, Opt. Commun. **35**, 451 (1980).

[20] A. Olsson, C. L. Tang, and E. L. Green, Appl. Opt. **19**, 1897 (1990).

[21] K. C. Smyth, R. A. Keller, and F. F. Crim, Chem. Phys. Lett. **55**, 473 (1978); K. C. Smyth and P. K. Schenck, *ibid.* **55**, 466 (1978).

[22] L. Allen and J. H. Eberly, *Optical Resonance and Two-Level Atoms* (Wiley, New York, 1975); R. J. Wilson and E. L. Hahn, Phys. Rev. A **26**, 3404 (1982).

[23] (a) R. J. LeRoy, J. Chem. Phys. **52**, 2678 (1969); (b) R. F. Barrow and K. K. Yee, J. Chem. Soc. Faraday Trans. 2 **69**, 684 (1973); (c) J. Tellinghuisen, J. Quantum Spectrosc. Radiat. Trans. **19**, 149 (1978).

[24] R. M. Bowman, M. Dantus, and A. H. Zewail, Chem. Phys. Lett. **15**, 131 (1989); Nature (London) **343**, 737 (1990); M. Grubele, G. Roberts, R. M. Bowman, M. Dantus, and A. H. Zewail, Chem. Phys. Lett. **166**, 459 (1990).

[25] K. F. Freed and A. Nitzan, J. Chem. Phys. **73**, 4765 (1980).

[26] G. Horlick, R. H. Hall, and W. K. Yuen, in *Fourier Transform Infrared Spectroscopy: Applications to Chemical Systems*, edited by J. R. Ferraro and L. J. Basile (Academic, New York, 1982), Vol. 3, Chap. 2, pp 37–81.

[27] M. Wang and A. G. Marshall, Anal. Chem. **60**, 341 (1988).

[28] "On resonance phase locking" for molecular I_2 refers to the empirical determination of the phase locked interferogram which exhibits the phase inversion feature at the largest time delay. Detuning is measured relative to the locked wavelength.

[29] E. J. Heller, J. Chem. Phys. **68**, 2066 (1978).

[30] L. D. Landau and E. M. Lifshitz, *Statistical Physics* (Pergamon, New York, 1980), Part 1, Ch. XII.

[31] C. Cohen-Tannoudji, B. Diu, and F. Laloe, *Quantum Mechanics* (Wiley, New York, 1977), Vol. 1, p. 559.

[32] The overlap function (4.21) can be easily obtained by operator algebra. It is calculated here via the wave function (4.19) in order to make clear its dependence on the position, momentum and phase of the propagated wave packet.

[33] This should not be misconstrued to imply that the Bv' level contributes more importantly to the fluorescence than other levels. For instance, because we assume the use of pulses with arbitrarily large spectral width, the center frequency may be most closely in resonance with a "level" having v' less than zero.

[34] M. Dantus, R. M. Bowman, and A. H. Zewail, Nature (London) **343**, 737 (1990).

[35] N. F. Scherer, A. Matro, L. D. Ziegler, R. J. Carlson, J. A. Cina, and G. R. Fleming (in preparation).

[36] N. F. Ramsey, *Molecular Beams* (Oxford University, New York, 1956); Phys. Rev. **78**, 695 (1950); M. M. Salour, Appl. Phys. **15**, 119 (1978); J. C. Bergquist, S. A. Lee, and J. L. Hall, Phys. Rev. Lett. **38**, 159 (1977).

[37] R. G. Brewer and R. L. Shoemaker, Phys. Rev. A **7**, 2105 (1973); R. G. Brewer and A. Genack, Phys. Rev. Lett. **36**, 959 (1976).

[38] See, for example, L. D. Zeigler, Y. C. Chung, P. Wang, and Y. P. Zang, J. Chem. Phys. **90**, 4125 (1989); J. S. Melinger and A. C. Albrecht, J. Phys. Chem. **91**, 2704 (1987); A. B. Myers, J. Opt. Soc. Am. B **7**, 1665 (1990); H. A. Ferwerda, J. Terpstra, and D. A. Wiersma, J. Chem. Phys. **91**, 3296 (1989).

[39] V. Romero-Rochin and J. A. Cina, J. Chem. Phys. **91**, 6103 (1989); J. A. Cina, Phys. Rev. Lett. **66**, 1146 (1991); J. A. Cina and V. Romero-Rochin, J. Chem. Phys. **93**, 3844 (1990).

[40] D. A. Wiersma and K. Duppen, Science **237**, 1147 (1987); K. Duppen and D. A. Wiersma, J. Opt. Soc. Am. B **3**, 614 (1986).

This article is copyrighted as indicated in the article. Reuse of AIP content is subject to the terms at: http://scitation.aip.org/termsconditions. Downloaded to IP: 128.32.208.2 On: Thu, 29 May 2014 17:58:57